Thesis

The intratumoral microbiome in primary and metastatic carcinomas of the aerodigestive tract.

submitted by

David Gorkiewicz

partial fulfillment of the requirements
for the degree of

Doktor der gesamten Heilkunde
(Dr. med. univ.)

at the

Medical University of Graz

executed at the

Diagnostic and Research Institute of Pathology

under the supervision of

Univ. FA Dr.med.univ. Martin Zacharias
Univ.-Prof. Dr.med.univ. Gerald Höfler

Graz, 11.03.2026

Declaration of academic integrity

I hereby confirm that the present diploma thesis is the result of my own independent scholarly work. I also confirm that in all cases, where material from the work of others (in books, articles, essays, dissertations, and on the internet) is acknowledged, quotations and paraphrases are clearly indicated. No material other than that cited in the reference list has been used. I have read and understood the Medical University's regulations and procedures concerning plagiarism.

Furthermore, I hereby declare that if artificial intelligence (AI) tools were used for the generation and/or correction of certain text passages in the creation of this work, such employment was conducted in compliance with ethical principles, academic integrity, and the regulations of my university. Additionally, it was ensured that this usage was transparently disclosed and appropriately attributed.

Graz, 11.03.2026 David Gorkiewicz m.p.

Acknowledgements

First and foremost, I would like to express my sincere gratitude to my supervisors, Univ.-FA Dr. med. univ. Martin Zacharias and Univ.-Prof. Dr. med. univ. Gerald Höfler. I would especially like to thank Martin for his guidance, encouragement and support throughout this project. His expertise, valuable feedback and continuous advice were essential for the completion of this work.

I am especially grateful to Christina Kumpitsch, PhD, and the entire team of the Moissl–Eichinger Lab for welcoming me so warmly into the laboratory and supporting me throughout the practical part of this project. Thank you for your patience in teaching me the laboratory methods and for always taking the time to answer my questions. The positive and supportive environment made working in the lab both an educational and enjoyable experience.

I am also deeply grateful to my parents, Gregor and Sabine Gorkiewicz, for their unconditional support over the years. They have always encouraged me to pursue my goals and gave me the opportunity to follow the professional path I had envisioned. Without their trust and encouragement, this journey would not have been possible.

Finally, I would like to thank some very special people for their support throughout this time. In particular, I would like to thank Magdalena Brugger, Raffael Geissler, Jordi Neumann and Michael Bertolli, as well as my siblings Sarah, Luna, Leon and Dorian and my grandmother Gundula for their understanding and for always being there for me. Their encouragement and the many moments of laughter along the way made this journey much easier.

Table of contents

Abbreviations

AGA	Actionable Genomic Alteration
ALK	Anaplastic Lymphoma Kinase
APC	Adenomatous Polyposis Coli
BRAF	B-Raf Proto-Oncogene
CAF	Cancer-Associated Fibroblast
CCL2	C–C Motif Chemokine Ligand 2
CDKN2A	Cyclin-Dependent Kinase Inhibitor 2A
CI	Confidence Interval
Cq	Quantification Cycle
CRC	Colorectal Carcinoma
CTNNB1	Catenin Beta 1
ddPCR	Droplet Digital Polymerase Chain Reaction
DNA	Deoxyribonucleic Acid
ECM	Extracellular Matrix
EGFR	Epidermal Growth Factor Receptor
EML4::ALK	Echinoderm Microtubule-Associated Protein-Like 4 – Anaplastic Lymphoma Kinase fusion
FFPE	Formalin-Fixed, Paraffin-Embedded
FGFR2	Fibroblast Growth Factor Receptor 2
FGFR3	Fibroblast Growth Factor Receptor 3
H&E	Hematoxylin & Eosin
HRAS	Harvey Rat Sarcoma Viral Oncogene Homolog
IARC	International Agency for Research on Cancer
KRAS	Kirsten Rat Sarcoma Virus
MMP	Matrix Metalloproteinase
MSI	Microsatellite Instability
NA	Not Assessed
ND	Not Detected
NGS	Next-Generation Sequencing
NK	Natural Killer (cells)
NSCLC	Non-Small Cell Lung Carcinoma
NTC	No-Template Control

PCR	Polymerase Chain Reaction
PIK3CA	Phosphatidylinositol-4,5-bisphosphate 3-kinase catalytic subunit alpha
PTEN	Phosphatase and Tensin Homolog
qPCR	Quantitative Polymerase Chain Reaction
ROS	Reactive Oxygen Species
rRNA	Ribosomal Ribonucleic Acid
SD	Standard Deviation
SMAD4	SMAD Family Member 4
SQ	Starting Quantity
STK11	Serine/Threonine Kinase 11
TGFβ	Transforming Growth Factor Beta
TME	Tumor Microenvironment
TNM	Tumor–Node–Metastasis Classification
TP53	Tumor Protein p53
VEGF	Vascular Endothelial Growth Factor
VLP	Virus-Like Particle
WHO	World Health Organization
WGS	Whole Genome Sequencing

List of figures

List of tables

Zusammenfassung

Einführung: Lungen- und kolorektale Karzinome zählen weltweit zu den häufigsten und tödlichsten malignen Erkrankungen. Dies verdeutlicht die Bedeutung eines besseren Verständnisses dieser Tumorentitäten und der Krebsbiologie insgesamt. Neben genetischen Mutationen rückt zunehmend das Tumormikromilieu in den Fokus, insbesondere die mögliche Rolle intratumoraler Mikroorganismen.

Methodik: Ziel dieser Arbeit war es, die bakterielle Last in archiviertem FFPE-Tumormaterial mittels 16S-basierter qPCR und droplet digital PCR (ddPCR) zu quantifizieren und mögliche Zusammenhänge mit histopathologischen Parametern sowie ausgewählten genetischen Mutationen zu untersuchen. Untersucht wurden 21 Tumorproben, darunter primäre kolorektale Karzinome, primäre Lungenkarzinome sowie pulmonale Metastasen kolorektaler Karzinome. Die verwendete DNA stammte aus Restmaterial der routinemäßigen molekularpathologischen Diagnostik. Zusätzlich wurden Nekrose, Muzingehalt und entzündliche Infiltration anhand von H.E.-Schnitten semiquantitativ evaluiert.

Ergebnisse: Die mittels qPCR und ddPCR bestimmten 16S-rRNA-Kopienzahlen korrelierten stark positiv miteinander (Spearman $r = 0.90$, $p = 0.0009$, $n = 10$). Im Vergleich zur qPCR erwies sich die ddPCR jedoch als sensitiver, insbesondere bei niedriger bakterieller DNA-Menge. In den Gruppenvergleichen zeigten kolorektale Karzinome die höchste und primäre Lungenkarzinome die niedrigste bakterielle Last. Lungenmetastasen wiesen signifikant höhere Nekroseanteile auf als die Primärtumoren. Eine signifikante negative Korrelation bestand zwischen der ddPCR-basierten bakteriellen Last und dem Ausmaß der entzündlichen Infiltration (Spearman $r = -0.65$, 95%-KI -0.85 bis -0.29, $p = 0.0015$, $n = 21$). Für die bakterielle Last und Nekrose, Muzingehalt sowie den Mutationsstatus von *KRAS*, *TP53* und *PIK3CA* ergaben sich keine signifikanten Zusammenhänge.

Diskussion: Ein methodischer Vorteil der Studie liegt in der Verwendung übriggebliebener DNA aus der Routinediagnostik, die aus seriellen Schnitten unmittelbar nach den histologisch beurteilten Präparaten gewonnen wurde. Dadurch war eine direkte räumliche Zuordnung zwischen molekularen und morphologischen Befunden möglich. Gleichzeitig zeigt die Arbeit, dass eine

bakterielle Quantifizierung grundsätzlich in bestehende diagnostische Abläufe integrierbar ist. Zusammenfassend belegt die Studie die Nachweisbarkeit intratumoraler bakterieller DNA in FFPE-Material und weist auf eine mögliche Interaktion zwischen bakterieller Last und tumorassoziierter Entzündung hin.

Abstract

Introduction: Colorectal and lung carcinomas are among the leading causes of cancer-related death worldwide, highlighting the need for a better understanding of these entities and cancer biology in general. The role of intratumoral microbiota in cancer biology has gained increasing attention in recent years. While tumor development has traditionally been linked to genetic and epigenetic alterations, it has become evident that the tumor microenvironment also includes microbial components. Intratumoral bacteria have been associated, among other factors, with immune cell infiltration, modulation of inflammatory pathways, tumor growth, and response to therapy. These findings suggest that tumor-associated microbiota represent an additional layer of biological complexity in cancer and that a better understanding of the tumor microenvironment (TME) is required to properly address these observations.

Methods and study design: This study aimed to quantify intratumoral bacterial load in archival FFPE tumor tissue using 16S quantitative PCR (qPCR) and droplet digital PCR (ddPCR) and to explore potential associations with histopathological features and selected genetic alterations. 21 tumor samples were analyzed, including primary colorectal carcinomas, primary lung carcinomas, and colorectal cancer metastases to the lung. DNA was obtained from residual material generated during routine molecular diagnostic procedures. Tumor necrosis, mucin content, and inflammatory infiltration were semi-quantitively assessed on hematoxylin–eosin–stained sections.

Results: 16S rRNA gene copy numbers measured by qPCR and ddPCR showed a strong positive correlation (Spearman r = 0.90, p = 0.0009, n = 10). Compared to qPCR, ddPCR demonstrated superior sensitivity, particularly in samples with low bacterial DNA abundance. In group comparisons, primary colorectal carcinomas exhibited the highest intratumoral bacterial load, whereas primary lung carcinomas showed the lowest levels. Lung metastases displayed significantly higher necrosis scores compared to primary tumors. A significant inverse association was observed between ddPCR-based bacterial load and the extent of inflammatory infiltration (Spearman r = −0.65, 95% CI −0.85 to −0.29, p = 0.0015, n = 21). No significant

associations were detected between bacterial load and necrosis, mucin content, or the mutational status of *KRAS*, *TP53*, and *PIK3CA*.

Conclusion: A particular strength of this study is the use of residual DNA derived from routine diagnostic workflows. DNA was extracted from serial FFPE sections directly following the histologically assessed slides, allowing spatial correlation between molecular and morphological analyses. This approach supports the potential integration of microbial quantification into standard pathological diagnostics without additional tissue processing. In summary, intratumoral bacterial DNA can be detected in FFPE tumor material using molecular techniques, with ddPCR providing superior sensitivity in low-biomass samples. The observed association between bacterial load and inflammatory infiltration suggests a potential interaction between tumor-associated microbiota and the immune microenvironment.

1. Introduction

1.1 Epidemiology of lung cancer and colorectal cancer

According to the most recent global cancer estimates published by the International Agency for Research on Cancer (IARC) through its GLOBOCAN 2022 database, lung cancer and colorectal cancer (CRC) together represent two of the most significant contributors to the worldwide cancer burden (1). Their combined impact accounts for a substantial proportion of global cancer incidence and mortality, reflecting both the prevalence of major risk factors and the challenges associated with early detection and effective treatment across different regions.

Lung cancer remains the most frequently diagnosed cancer globally, with approximately 2.5 million new cases reported in 2022, corresponding to 12.4% of all cancer diagnoses. It is also the leading cause of cancer-related death, responsible for an estimated 1.8 million deaths, or 18.7% of all cancer mortality (1). The persistently high incidence rate reflects the strong association between lung cancer and modifiable exposures such as tobacco smoking, which remains the dominant risk factor worldwide. Additional contributors include air pollution, occupational carcinogens (e.g., asbestos, silica dust) and indoor pollutants (2). Many cases are diagnosed at an advanced stage, which further contributes to poor survival outcomes (3). Colorectal cancer (CRC) represents another major global public health challenge. In 2022, approximately 1.93 million new cases were registered worldwide, making it the third most common cancer (after lung and breast cancer), accounting for 9.6% of all cancer diagnoses. CRC was responsible for around 900,000 deaths (9.3% of all cancer deaths), ranking it among the leading causes of cancer mortality (1). Colorectal cancer is closely associated with dietary and lifestyle factors, such as high consumption of red and processed meat, obesity, sedentary lifestyle, alcohol consumption, and smoking. Importantly, CRC is largely preventable and detectable through screening, which significantly lowers mortality when widely implemented (4).

Together, lung and colorectal cancer accounted for approximately 4.4 million new cases and 2.7 million deaths in 2022, representing 22% of all cancer diagnoses and nearly 28% of all global cancer deaths (1). This combined burden underscores the magnitude of these two cancers in shaping global cancer epidemiology.

There are substantial geographical variations. Lung cancer incidence is highest in regions with a history of heavy tobacco use, including Europe, East Asia, and parts of North America, but it is increasingly affected by air pollution in densely populated Asian countries. Colorectal cancer incidence is highest in high-income countries such as Australia, New Zealand, the United States, Japan, and several Western European nations, reflecting dietary patterns, obesity rates and lifestyle factors. Asia, due to its population size, accounts for the greatest number of total CRC cases and deaths, despite lower age-standardized rates in many countries (1,3). Hungary has the highest age-standardized incidence rate (ASIR, 47.6 per 100,000) and the highest age-standardized mortality rate (ASMR, 39.8 per 100,000) for lung cancer worldwide. In CRC, Denmark has the highest reported ASIR (48.1), whereas Hungary also shows the highest ASMR (20.2) among individual countries (1). Notably, a recent population-based study has shown that colorectal cancer incidence in Denmark increased after the introduction of a national screening program in 2014. This observation suggests that improved detection through systematic screening may partially explain the comparatively high reported incidence rates (5). Age-standardized lung and colorectal cancer incidence and mortality rates per 100 000 of both sexes in 2022 are shown in Figure 1 and Figure 2.

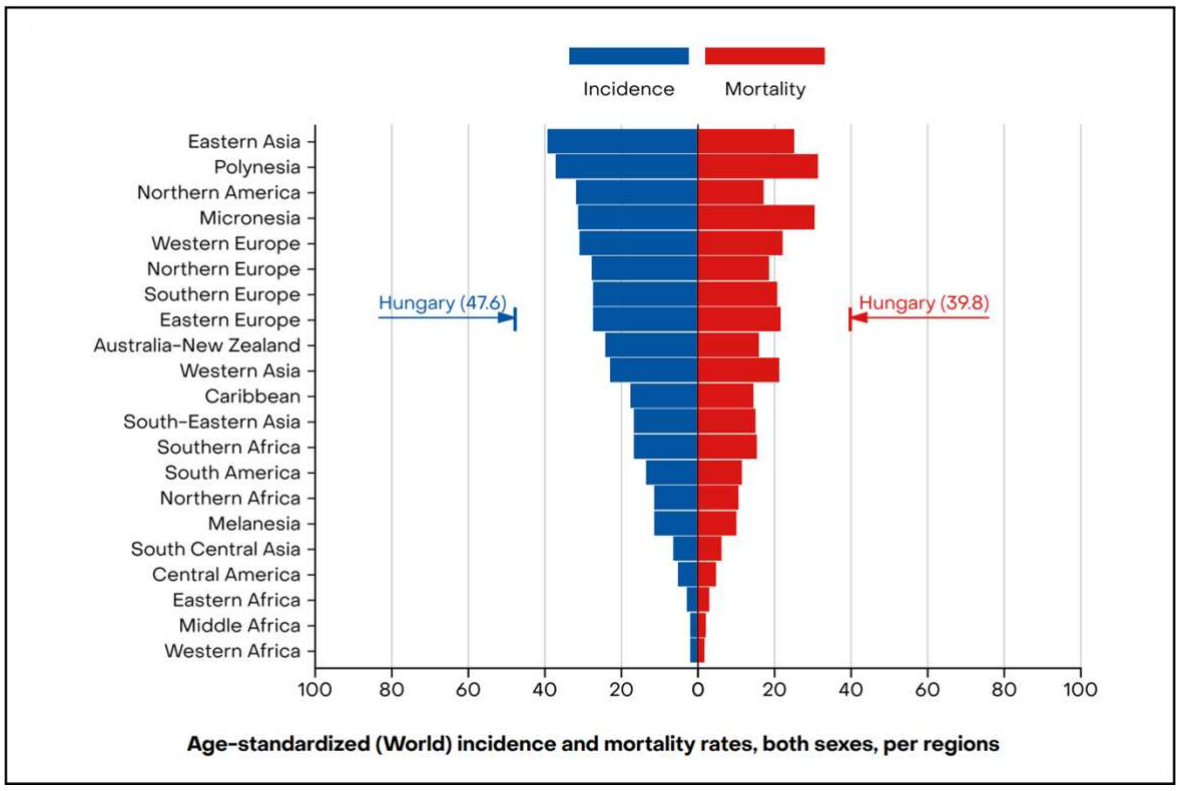

Figure 1: Lung cancer incidence and mortality rates per 100 000 of both sexes. From: GLOBOCAN 2022 (1)

IARC projections suggest a significant rise in both lung and colorectal cancer by 2040. Population ageing, increased life expectancy, urbanization and the global spread of “westernized” lifestyle patterns are expected to drive further increases in CRC incidence, particularly in middle-income countries (1,4). A concerning trend is the growing incidence of colorectal cancer in younger adults, especially in high-income regions, for reasons that are not yet fully understood (4). For lung cancer, trends will largely depend on global tobacco control policies and environmental interventions targeting air pollution (3).

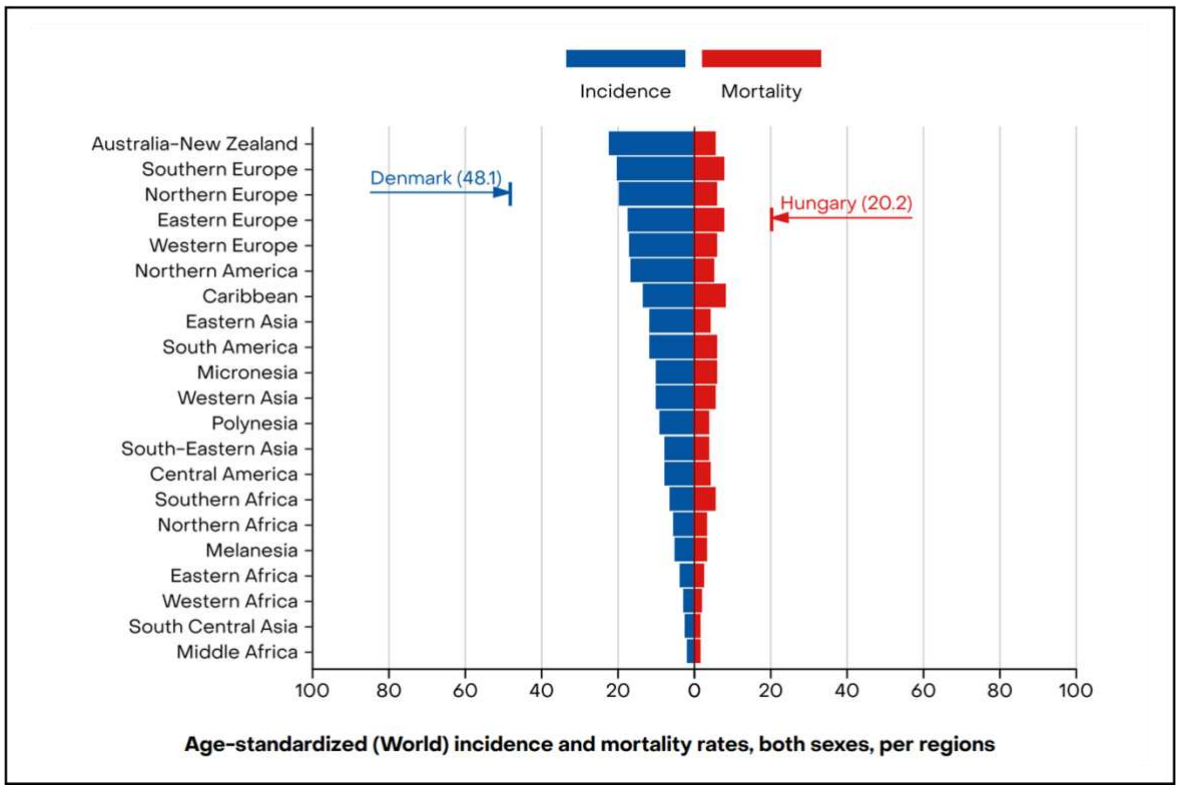

Figure 2: Colorectal cancer incidence and mortality rates per 100 000 of both sexes. From: GLOBOCAN 2022 (1)

1.2 Clinicopathological background of lung cancer

1.2.1 Clinical features of lung cancer

Symptoms of lung cancer include cough, dyspnea, chest pain, hemoptysis, recurrent pneumonia and paraneoplastic syndromes. Because patients often remain asymptomatic for long periods, lung cancer is frequently diagnosed at an advanced stage. Staging of lung cancer relies on thoracic computed tomography (CT), cerebral magnetic resonance imaging (MRI) and, where appropriate, fluorodeoxyglucose positron emission tomography (FDG-PET) imaging and endobronchial ultrasound-guided transbronchial needle aspiration (EBUS-TBNA) (6). Lung cancer can be divided into two major categories: non-small cell lung carcinoma (NSCLC) and small cell lung carcinoma (SCLC) (7). While SCLC was historically classified as limited or extensive disease, both NSCLC and SCLC are currently staged according to the TNM classification system (8).

1.2.2 Histologic classification of lung cancer

NSCLC represents the largest group and includes adenocarcinoma, squamous cell carcinoma and large cell carcinoma, along with several less common variants such as adenosquamous carcinoma, sarcomatoid carcinoma and large cell neuroendocrine carcinoma (LCNEC)(7). Adenocarcinomas can be further divided into 5 main histologic growth patterns: papillary, micropapillary, acinar, lepidic and solid (Figure 3). Additionally they can be classified as mucinous and nonmucinous subtypes (9). Lung adenocarcinoma most commonly metastasizes to the brain, followed by bone, liver, and adrenal glands (10). The most frequent genetic alterations include *EGFR* mutations (10–15%), *KRAS* mutations (20–25%) and *ALK* rearrangements (approximately 4%) (11–13).

SCLC is classified as a distinct, high-grade neuroendocrine carcinoma and can be further divided at the molecular level based on dominant transcription factors (14,15). The WHO also defines pulmonary neuroendocrine tumors as a separate major category, comprising typical carcinoid, atypical carcinoid, LCNEC and SCLC. Globally, NSCLC accounts for approximately 85–89% of all lung cancer cases, with adenocarcinoma being the most frequent subtype (39–57%), followed by squamous cell carcinoma (12–25%) and large cell carcinoma (6–8%). SCLC represents about 9–14% of cases, while pulmonary carcinoid tumors constitute less than 2% of all lung cancers (16–18).

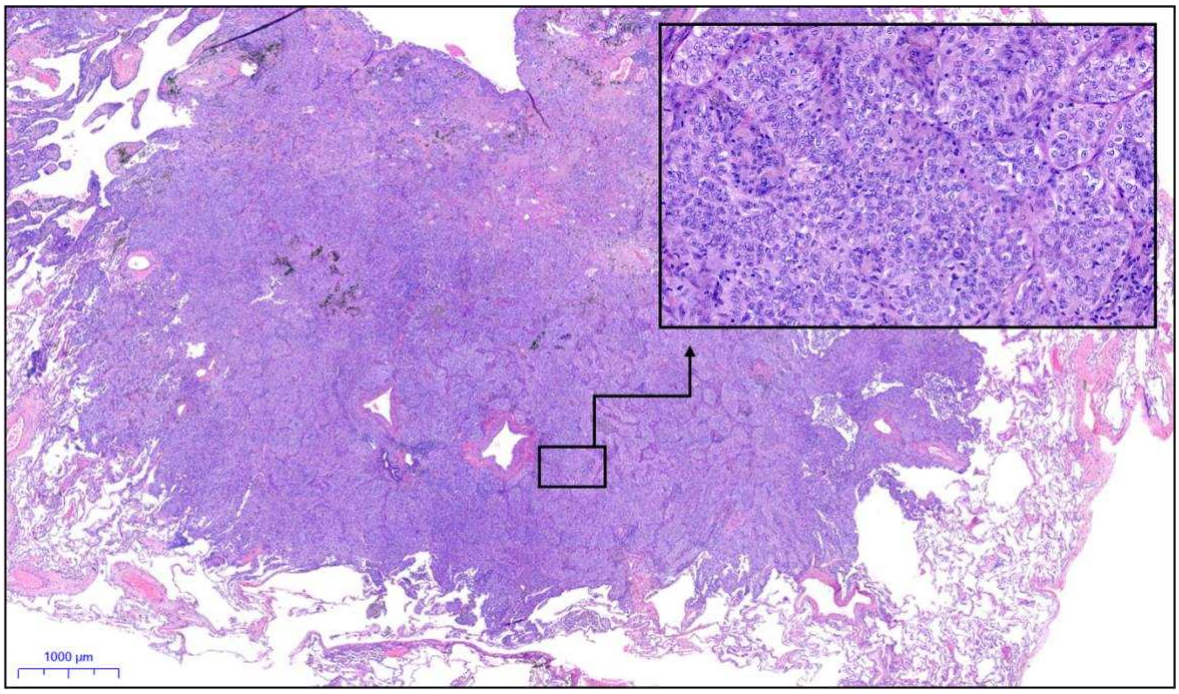

Figure 3: Histological H&E-stained section of a solid primary lung adenocarcinoma. Inset highlights solid histoarchitecture of the carcinoma.

1.2.2 Lung metastases

Notably the lung is also a common site for metastasis. 50% of metastasic cancer patients develop lung metastases which are associated with poor clinical outcome and significantly compromise quality of life (19). The colon and rectum are the most common primary sites from which lung metastasis originates, followed by the kidney, breast and pancreas (20).

1.3 Clinicopathological background of colorectal cancer

1.3.1 Clinical features of CRC

Symptoms of CRC include constipation, diarrhea, rectal bleeding, hematochezia, unexplained weight loss and abdominal pain. Early detection and removal of the precancerous lesion (in most cases an adenomatous polyp) via colonoscopy is necessary for surveillance, adequate diagnosis, prognosis and treatment. CRC can be divided into two main categories, depending on anatomical site: right sided CRC (RCRC) if it is located in the ascending or transverse colon, left sided CRC (LCRC) if it is situated in the descending-/sigmoid colon or the rectum. RCRC is associated with larger, higher grade and stage tumors as well as worse overall survival rate

than LCRC. The site of origin is also affecting characteristics like the immunologic response, the specific molecular aberrations and clinical presentation (21).

1.3.2 Histologic classification of CRC

Histopathologically, adenocarcinoma is the most common type of CRC, accounting for approximately 90–95% of all cases (22). CRC most commonly metastasizes to regional lymph nodes, liver, peritoneum, lung, and ovaries (23). The most frequently mutated genes of adenocarcinomas of the colon include *APC*, *TP53*, and *KRAS* (24). According to Fleming et al, well-differentiated (low-grade) adenocarcinomas are characterized by abundant, well-formed epithelial glands, accounting for more than 95% of the tumor area. Moderately differentiated adenocarcinomas, which represent the majority of cases at diagnosis, display recognizable gland formation in approximately 50–90% of the tumor. In contrast, poorly differentiated (high-grade) adenocarcinomas exhibit gland formation in less than 50% of the tumor (25). The WHO recognizes six histological subtypes of adenocarcinoma: mucinous, signet ring, serrated, micropapillary, cribriform-comedo and medullary (21,22). Mucinous adenocarcinomas (Figure 4) account for approximately 17% of CRC. These tumors contain extracellular mucin retained within the tumor mass. Around 2-4% of mucinous CRC store mucin intracellularly that pushes the nucleus to the side, producing the typical signet-ring morphology (22). Mucinous CRCs are most commonly found in the right colon and are often diagnosed at a high stage (26). They tend to metastasize to the peritoneum rather than the liver and demonstrate reduced responsiveness to therapy. Mucinous adenocarcinomas are characterized by distinct molecular features, including microsatellite instability (MSI) as well as an increased frequency of *KRAS*, *BRAF* and *PI3K* mutations (26,27). Other rare epithelial tumor variants are squamous cell carcinomas, spindle cell carcinomas and adenosquamous carcinomas. In addition, there are undifferentiated carcinomas, which lack glandular structures and other distinguishing features such as mucin production. Other types of colon tumors are non-epithelial like lymphoid or haemopoietic neoplasms, gastrointestinal stromal tumors (GISTs), leiomyosarcomas or neuroendocrine tumors (NETs) (21,22).

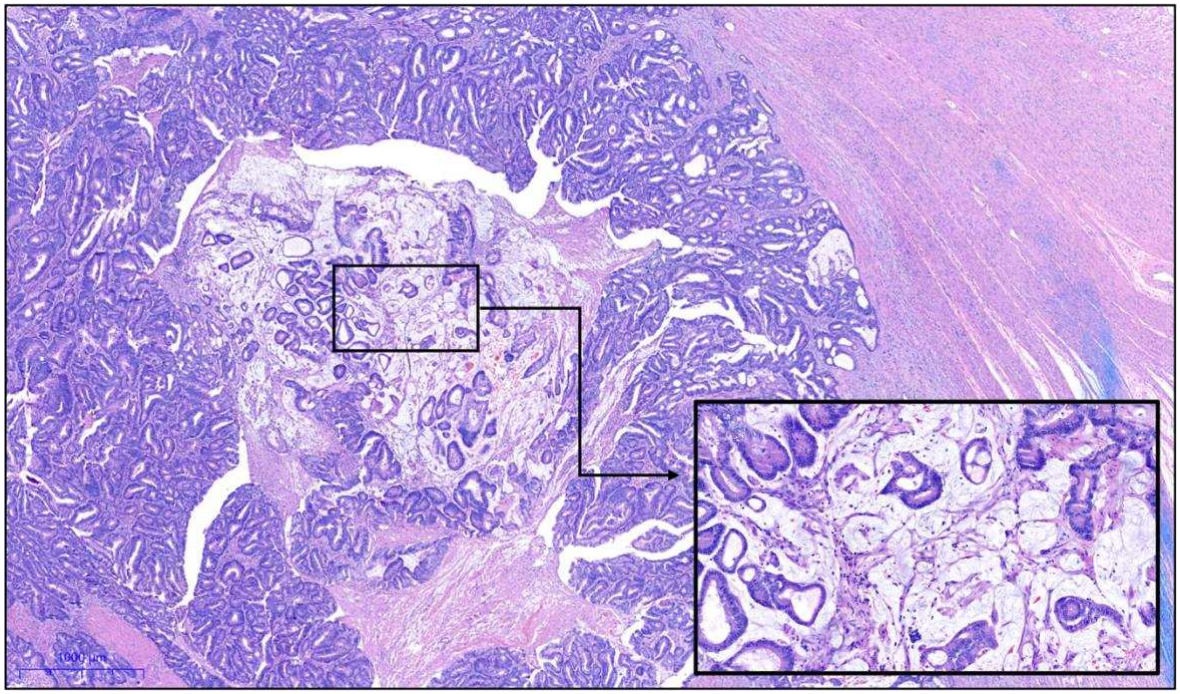

Figure 4: Histological H&E-stained section of a mucinous primary colon adenocarcinoma. Inset depicts mucinous histoarchitecture.

1.4 The UICC TNM classification

Both lung cancer and CRC are classified according to the Union for International Cancer Control (UICC) TNM staging system (8,21,28). Clinical staging describes the extent of disease at diagnosis and is based on clinical assessment, imaging and diagnostic biopsies prior to treatment. In patients undergoing surgical resection, an additional pathological stage can be assigned based on postoperative histological evaluation. Both clinical and pathological staging assess the primary tumor (T), regional lymph node involvement (N) and the presence of distant metastases (M). These categories are subsequently combined into stage groups I–IV, with stage I disease confined to the organ of origin and stage IV indicating distant metastatic spread (29). The TNM classification is used to guide treatment planning, estimate prognosis, enable standardized communication across centers and support cancer research and control efforts (30).

1.5 Molecular diagnostics

Molecular diagnostic approaches such as immunohistochemistry (IHC), fluorescence in situ hybridization (FISH) and PCR-based assays for the detection of point mutations are well established in routine cancer diagnostics. For many years, genetic profiling of tumors has primarily relied on single-gene assays. These assays typically focus on a small set of genes of known oncogenes (e.g., *HER*, *RAS*, *MET*) or tumor-suppressor genes (e.g., *APC*, *TP5*3, *BRCA*) and are not able to detect mutations in non-coding regions. With such assays, clinicians might miss opportunities for treatment options or early detection of cancers (31,32). NGS, including whole-genome sequencing (WGS), has been adopted to address these issues. Sequencing entire cancer genomes enables identification of various genetic alterations and therefore is crucial in implementing precise treatment, tailored to the specific genetic profile of the tumor and can serve as a prognostic marker (31). Although NGS offers clear advantages over single-gene assays, its widespread implementation remains limited, largely due to its high costs (33).

In 2004, Lynch et al. proclaimed that a mutation in the epidermal growth factor (*EGFR*) leads to NSCLC responsiveness to Gefitinib, therefore identifying the first actionable genomic alteration (AGA) in lung cancer (34,35). Common *EGFR* mutations are exon 19 deletions and exon 21 L858R. Other AGAs in NSCLC are *BRAF* V600E, *MET* Exon 14-skipping or *KRAS* G12C mutations (35). In SCLC, tissue availability is often limited. Although transcriptional profiling has recently enabled molecular subtyping of SCLC, the clinical relevance and therapeutic implications of these subtypes are not yet fully established. Genomic alterations of *TP53*, *RB1*, *PIK3CA* and *PTEN* as well as alterations activating the PI3K/Akt/mTOR pathway can be found in SCLC (36).
In CRC, mutations of *APC*, *TP53*, *PIK3CA*, *BRAF* (e.g.,V600E) and *KRAS* (e.g., G12C) can be frequently found (37). Interestingly, genetic profiles differ substantially when comparing anatomical sites. For example a higher frequency of *BRAF*, *RAS* and *PIK3CA* mutations has been reported in right-sided colorectal cancers relative to left-sided tumors (38).

1.6 Tumor microenvironment (TME)

In recent years, the tumor microenvironment (TME) has gained increasing attention in cancer research, as it plays a crucial role in tumor development, progression and metabolism. Although the precise impact of bacteria, fungi and viruses on the TME is not yet fully understood, increasing research in this area has already provided important insights into how microbial communities may shape cancer biology. The term “TME” first got introduced in 1889 through the “seed & soil”-hypothesis by Steven Paget which proclaims that cancer cells emerge in microenvironments most suitable for their growth (39).

Today, we understand the TME as an intricate interplay of both cellular and non-cellular components. Involved cell types include immune cells, endothelial cells and cancer associated fibroblasts (CAFs). These cells produce a wide spectrum of soluble factors such as chemokines, cytokines, metabolites, signaling molecules and extracellular vesicles (40). Non-cellular elements include the extracellular matrix (ECM), interstitial fluid, electrolytes and nutrients, all of which together contribute to the dynamic composition of the TME (41,42).

Interestingly, the interplay between cancer cells and their microenvironment is bidirectional: the composition and behavior of the microenvironment influences cancer cells, while cancer cells in turn shape the surrounding microenvironment (43). For example, in metastatic cancer, factors like TGFβ, VEGF and CCL2 are secreted by the tumor cells and drive lung metastasis through intricate interactions that promote immune cell recruitment, ECM modulation and angiogenic remodeling. Furthermore, tumor-derived exosomes and microparticles influence organotropism and suppress immune responses by modifying the lung microenvironment. Together, these changes establish a pre-metastatic niche that facilitates tumor cell colonization and growth (19).

1.7 Specialized microenvironments within the TME

One modern approach of defining the TME is to divide it into a system composed of 6 specialized microenvironments: immune, metabolic, hypoxic, acidic, mechanical and innervated, each contributing uniquely to tumor behavior (44).

The immune microenvironment contains various types of different immune populations including macrophages, dendritic cells, NK-cells, neutrophils and T-/B-lymphocytes which produce a variety of substances like chemokines, extracellular vesicles and cytokines. These cells sometimes have opposing functions like promotion or suppression of cancer progression which highlights the complexity of this compartment (45,46).

The metabolic microenvironment is made of different metabolites that the tumor cells or the cells within the TME produce like lactate, glucose, reactive oxygen species or amino acids (47). As an example, tumor cells rely heavily on glycolysis and generate lactate even when oxygen is sufficient, a process known as the “Warburg effect” (48). Consequently, the TME becomes enriched with lactate while glucose levels decline, practically “starving” other cells like T-cells that rely heavily on glucose. The TME is also characterized by elevated levels of reactive oxygen species (ROS), largely generated by tumor cells who also possess enhanced mechanisms to tolerate oxidative stress, giving them a survival advantage over other cell types (44).

The hypoxic microenvironment, as its name indicates, describes niches within the tumor that have insufficient oxygen supply. The reason for this is the inadequate vascularization of the tissue due to the unregulated tumor cell proliferation. This leads to increased aggressiveness of cancer cells due to hypoxia-triggered reprogramming and serves as a negative prognostic marker (44).

The acidic microenvironment describes the mildly acidic niche in which the tumor thrives. Its pH values are usually between 6.7 and 7.1 and are a consequence of the metabolic and hypoxic microenvironment, largely due to the production of lactate (44).

The mechanical microenvironment contains the extracellular matrix within the TME including various cell types like CAFs, osteoblasts and mesenchymal stroma cells that form a dense network around the tumor (49). The increased production and remodeling rate of the tumor stroma leads to its stiffness which is largely driven by CAFs and special enzymes like metalloproteinases (MMPs), hyaluronidases or elastases (50). Tumor cells coordinate cell/cell adhesions, primarily mediated by E-cadherin, with cell/matrix adhesions through integrins which enables them to migrate, invade surrounding tissue and spread to other sites (44).

The innervated microenvironment is the entirety of nerval structures within the TME. The tumor secretes molecules like neurotrophins that promote peripheral nerve infiltration and neuronal stem cell migration. The neurons within the TME further produce neuropeptides and neurotransmitters that drive tumor progression. Another feature of this TME niche is perineural invasion which is associated with the metastasis along peripheral nerves to distant sites (51).

1.8 The human microbiome

Given that the TME is highly responsive to external and internal influences, microbial factors have recently moved into focus as potential modulators. The human body contains approximately 4×10^{13} microbial cells spanning ~3×10^{3} species. The vast majority of microbial cells (>90%) are located in the gut, while smaller communities inhabit the skin, respiratory and uro-genital tracts (52,53). The human microbiome contains bacteria, fungi and archaea but also viruses and phages. Virus-like particle (VLP) counts suggest that virus numbers are comparable to bacterial and human cells, with virus-to-bacteria ratios ranging roughly from 0.1 to 10 (54). It is important to note that there are substantial differences in microbial abundance and species composition not only between hosts, but also within a single host, depending on factors such as anatomical site, age and dietary habits (55–57).

The bacteria associated with the gut microbiome are largely composed of 6 phyla: *Firmicutes*, *Bacteroidetes*, *Verrucomicrobia*, *Proteobacteria*, *Fusobacteria* and *Actinobacteria* (58). The dominant fungi in the gut are *Mallassezia*, *Saccharomyces*, *Candida* and *Cladosporium* (59). Apart from these most abundant species in the gut

is M*ethanobrevibacter smithii* which represents an archaea (60). The unique metabolic genes and the enzymes they microbiome encodes enable the human body to digest and extract additional nutrients and energy from food. They also enable us to produce bioactive molecules like lipids, vitamins and amino acids. Furthermore, the gut microbiome has a big influence on host immunity. For instance, by producing antimicrobial compounds and by supporting the development of the intestinal mucosa, shielding us from colonisation of pathogenic microbes and by "training" our immune system. *Bifidobacterium* for example actively stimulates our immune system. With age, abundances of certain beneficial microbes in our gut decline which is associated with a higher chance of inflammation. The oral microbiota is another important niche and consist largely of *Fusobacteria*, *Proteobacteria*, *Bacteroidetes*, *Actinobacteria* and *Firmicutes* (55). The core lung microbiota contains *Firmicutes*, *Actinobacteria*, *Bacteroidetes* and *Proteobacteria* even though it the healthy lung was considered to be sterile for a long time (61,62). The anatomy of the skin and alongside its chemical composition leads to a distinct spatial "biogeography" of the microbiota. In general, it contains *Proteobacteria*, *Actinobacteria*, *Bacteroidetes* and *Firmicutes*. Dysbiosis of the skin microbiome can contribute to various skin disorders, such as acne, which is mediated in by the colonization of *Cutibacterium acnes* (55,63).

1.9 Microbes in cancer

Because microbes play such fundamental roles in host physiology and disease development, it is plausible that they also affect oncogenesis, tumor growth, metastasis and responses to cancer therapy. Accounts of studies about how bacteria may influence tumors date back to 1550 BCE and the Ebers Papyrus. The Egyptian physician Imhotep proclaimed that a treatment with poultice helps against tumors ("swellings") when combined with an incision, causing an inflammation (64). Peregrine Laziosi, an Italian monk who lived in the 13th century, described spontaneous regression of his bone cancer after it broke through the skin and got infected, which led to his canonization in 1609. At the end of the 1800s, both Wilhelm Busch and Friedrich Fehleisen reported instances where Streptococcus pyogenes infections appeared to trigger spontaneous regression of tumors (65).

The concept of oncogenic viruses originated from the pioneering work of Peyton Rous in 1911, who described a filterable agent, later identified as Rous sarcoma virus (RSV), in chicken sarcoma tissue that induced tumor formation when transmitted to healthy chickens (66). In 1964, Epstein et al discovered a virus (HHV-4, EBV) in Burkitt's Lymphoma cells (67). Hepatitis B virus (HBV) was discovered in 1970 and later linked to hepatocellular carcinoma development through epidemiolocal studies (68,69). The association between human papillomavirus (HPV) infection and cervical cancer was first proposed by Harald zur Hausen in 1977 and was subsequently confirmed by the identification of high-risk HPV types, particularly HPV16 and HPV18, in cervical carcinoma cells (70,71). Harald zur Hausen was awarded the Nobel Prize in Physiology or Medicine in 2008 for this discovery (72). In 1983, Robin Warren and Barry Marshall successfully cultured *Helicobacter pylori*, which subsequently led to epidemiological and experimental studies establishing its causal role in gastric carcinogenesis (73,74).

In 2018, infectious agents were estimated to account for approximately 13% of all global cancer cases (≈2.2 million), with viral infections contributing about 9.9%, bacterial infections about 4.0% and parasitic infections approximately 0.3% (75). The IARC classifies potential carcinogens into groups based on the strength of scientific evidence. Group 1 carcinogens are agents for which clear evidence of carcinogenicity in humans exists. This group comprises HPV, HBV, hepatitis C virus (HCV), EBV, human T-cell lymphotropic virus type 1 (HTLV-1), Kaposi sarcoma–associated herpesvirus (KSHV) and Merkel cell polyomavirus. Group 1 also includes the bacterium *Helicobacter pylori* and the parasitic helminths *Schistosoma haematobium*, *Opisthorchis viverrini* and *Clonorchis sinensis* (76).

However, carcinogenesis is not exclusively driven by individual oncogenic taxa. Increasing evidence suggests that alterations in the overall microbial composition and load of the gut can indirectly contribute to tumor development and progression at distant sites, including lung-, pancreatic- and breast cancer. Proposed mechanisms include microbial genotoxin production, chronic systemic inflammation and modulation of immune surveillance (77–79).

1.10 Molecular characterization of intratumoral bacteria

Thus, the theory of bacteria somehow influencing cancer biology is not new. What is new, however, is the ability to study these interactions at the molecular level. With the invention and broad accessibility of PCR techniques, characterization of the microbiome and detection of bacteria in tumors, including precise identification of their species, became possible. Nejman et al. analyzed the bacteria in 1010 tumor samples from melanoma, ovarian, lung, pancreatic, bone and breast cancers as well as glioblastoma. They used several techniques, including cultivation, electron microscopy, qPCR, multi-region 16S rRNA amplicon sequencing, immunofluorescence and immunohistochemical staining for lipopolysaccharide (LPS) and lipoteichoic acid (LTA). To account for potential contamination, 811 control samples from DNA extraction, PCR amplification and paraffin embedding were analyzed, resulting in the removal of 94.3 percent of bacterial signals as artifacts. The remaining signals came from 528 bacterial species that differed in composition, diversity and predicted metabolic properties across tumor types. Histologic imaging further demonstrated a heterogeneous spatial distribution of bacteria and intracellular localization within both tumor and immune cells (80).

Although tumor-associated microbiota has been intensively investigated in recent years, its existence remains controversial. Gihawi et al. analyzed microbial communities from 8,908 patients across 22 cancer types using whole-genome sequencing data from the Genomics England cohort and demonstrated that, among the analyzed entities, only colorectal cancer exhibits a distinct tumor-associated microbial signature that can be clearly distinguished from the surrounding anatomical site (81).

1.11 Ribosomal RNA genes and the 16S rRNA marker

To enable broad-spectrum detection of bacteria, molecular approaches targeting ribosomal RNA genes have been developed. In most bacteria, the 16S, 5S and 23S rRNA genes typically form a chromosomal rRNA operon, although in some species they can also be located on plasmids (82). These genes are responsible for rRNA synthesis which together of several proteins are the structural components of ribosomes, the organelles responsible for protein biosynthesis. Both prokaryotic and

eukaryotic ribosomes consist of two major subunits: a small subunit and a large subunit. In prokaryotes (bacteria and archaea), the 30S small subunit contains the 16S rRNA along with 21 associated proteins, while the 50S large subunit comprises two rRNAs (5S and 23S) and 31 proteins (83).

The 16S, 5S and 23S rRNA genes are universally present in all self-replicating life forms and shows slow sequence divergence (84). In 1965 Dubnau et al. reported that 16S rRNA gene sequence relationships are conserved across *Bacillus* spp. (85). This remarkable level of conservation likely arises from its critical function in bacterial survival (86). In 1987 Carl R. Woese described the rRNA genes as a molecular chronometer due to their universal presence, heterogeneous evolutionary rates across sequence regions, structural complexity and practical accessibility for direct sequencing thus making them the perfect phylogenic marker (87). The 16S rRNA gene is approximately 1500 base pairs long which makes it long enough to provide phylogenetic information while remaining short enough for efficient molecular analysis. The 16S rRNA gene contains ten conserved regions (C1–C10) that serve as reliable targets for primer design, enabling amplification of the intervening hypervariable regions. In contrast, the nine variable regions (V1–V9) harbor most of the phylogenetic and taxonomic information. Sequences from *Escherichia coli* are commonly used as a reference framework for defining nucleotide positions and for naming primers (88).

1.12 PCR technologies

1.12.1 Conventional PCR

Amplification of genetic material is essential for most molecular analyses because nucleic acids are often present in very low amounts in biological samples. The term „Polymerase chain reaction“ (PCR) describes a enzymatic amplification of genetic material and was first used by Saiki et al. in 1985 (89). But it took another 3 years until the utilization of a heat-resisting polymerase from *Thermus aquaticus* (Taq-polymerase) enabled routine usage of the PCR. The previously used polymerase had to be added after every denaturation step because it got deactivated by the heat. Containing primers, DNA polymerase, nucleotides, specific ions and a DNA

template and involving repeated cycles of DNA denaturation, primer binding and strand extension, the fundamental concept has remained unchanged since 1985. This groundbreaking invention propelled research across numerous scientific fields and significantly expanded the collective body of knowledge (90).

1.12.2 Quantitative PCR (qPCR)

The next milestone was the invention of quantitative PCR (qPCR) which is a procedure first described by Higuchi et al. in 1992 (91). The qPCR or real-time PCR is a method where the amplifications within the PCR process are monitored in real time with the help of fluorescence. After each circle, the fluorescence is measured and its intensity grows proportionally to the number of amplicons in the sample. The point at which the fluorescence intensity is high enough to distinguish it from the background is called quantification cycle (Cq) and allows determination of the initial number of template DNA or RNA molecules in the sample if compared to a calibration curve of serially diluted standard samples (90).

1.12.3 Digital droplet PCR (ddPCR)

The term “digital PCR” was first introduced by Vogelstein and Kinzler in 1999 to describe a method in which a DNA sample is partitioned into multiple individual PCR reactions such that single target molecules are amplified independently. By scoring reactions as positive or negative and applying Poisson statistics, this approach enables absolute quantification and highly sensitive mutation detection. (92) In contrast to real-time PCR, digital PCR does not rely on amplification kinetics or standard curves, thereby providing improved precision, robustness and accuracy, particularly for low-abundance targets. However, this method was limited by the small number of available reaction partitions, resulting in restricted dynamic range, low throughput and increased sample consumption. In 2011, Hindson et al. described a method called “droplet digital PCR” (ddPCR) in which individual target molecules are amplified within single water-in-oil droplets, thereby enabling a cost-effective, high-throughput implementation of digital PCR with low cross contamination. By partitioning a 20 µL reaction mixture into approximately 20,000 monodisperse droplets, each droplet functioned as an independent PCR microreactor (93). Based on this microfluidic technique, many ddPCR systems have

been developed in the last few years. However ddPCR is still far from being as universally available as qPCR due to its higher costs (94).

1.13 Impact of microbiota on the TME and therapy

It is known that microorganisms can influence the TME and cancer treatment. Various studies have shown its involvement in chemotherapy, radiotherapy and immunotherapy (95–102). Fecal and tissue microbiota, including *Fusobacterium*, *Blautia* and *Faecalibacterium,* are associated with T-cell infiltration and mesenteric lymph node involvement in CRC patients (103). *Bifidobacterium* species have shown to suppress CRC growth by altering the immune profile of the TME which enhance the efficacy of immune checkpoint inhibitors and emphasizes the potential of probiotics as a complementary treatment to immunotherapy. *Bifidobacterium adolescentis* was found to be decreased in CRC samples. When this strain was induced in CRC mouse models, a subpopulation of CAFs emerged within the TME which ultimately led to tumor suppression. On the other hand, *Fusobacterium nucleatum* can disrupt the tumor cell E-cadherin/β-catenin axis within the TME which promotes increased invasiveness of CRC cells (44).

In murine melanoma models, both the translocation of the intestinal commensal *Lactobacillus reuteri* to the tumor site and its direct intratumoral administration were found to enhance the type 1 cytotoxic T cell (Tc1) phenotype within the tumor microenvironment, thereby suppressing tumor progression. This effect was mediated by *L. reuteri*-derived indole-3-aldehydes (I3As), which activated aryl hydrocarbon receptor (AhR) signaling in $CD8^+$ T cells. Activation of the AhR pathway subsequently promoted interferon-gamma (IFNγ) secretion, leading to higher antitumor immune activity (104).

1.14 Bacteria-based therapeutic strategies in cancer

The natural tumor tropism of bacteria leads to various therapy options where cytotoxic substances can be delivered directly to the tumor by bacteria within the TME. One approach is the intracellular delivery of antitumor agents via phagocytosis of the bacteria. Another way is the use of bacteria that produce and release these cytotoxic substances extracellularly while residing inside the TME. Programmed bacterial lysis is also a modern approach and enables the production/release of

cytotoxic material only when the desired bacterial population density has been reached which leads to reduced bacterial load and danger of systemic side-effects (65). Din et al. used non-pathogenic *Salmonella* and *E.coli* strains that were engineered to lyse at a specific population threshold and produce a hemolysin, a chemokine and a pro-apoptotic protein (105). Chowdhury et al. later evolved this design to deliver antibody-fragments against CD47. Tumor cells sometimes overexpress CD47 to escape dendritic cell phagocytosis. Interestingly, this triggered a tumor-antigen-specific CD8+ T cell response that prevented metastasis and reduced even distal tumors that have not been injected. The mice used in this trial also had no anemia or thrombocytopenia which is otherwise common in CD47 expressing tumors (106).

2. Aims of this thesis

First, this thesis aims to provide an overview of the current state of knowledge of the tumor microbiome. In its practical part, it investigates the performance of the bacterial quantification methods 16S qPCR and 16S ddPCR in evaluating the bacterial load within different tumor microenvironments. The analysis is based on 21 tissue samples of colorectal cancer, lung cancer and colorectal cancer metastases to the lung. In addition, semi-quantitative histological scoring is employed to explore potential associations between necrosis, mucin content, inflammatory features and the abundance of intratumoral bacterial communities. Furthermore, intratumoral bacterial load is compared with the mutation status of selected cancer-related genes to assess potential associations between microbial burden and genetic alterations.

3. Material and methods

In this study, we included 21 tumor samples with associated residual, already routinely extracted tumor DNA. All samples originated from surgically resected tumor specimens. Following surgical resection, specimens were fixed in 4% neutral-buffered formalin and paraffin-embedded. Formalin-fixed, paraffin-embedded (FFPE) tumor tissue blocks were used for molecular diagnostic testing at the time of initial histopathological work-up. DNA was extracted from FFPE tissues using the Maxwell 16 Tissue DNA Purification Kit (Promega). DNA concentration was measured by PicoGreen fluorescence (107). All the steps described were performed in accordance with standard routine protocols at the Diagnostic and Research Institute of Pathology, Medical University of Graz. DNA remaining from these routine molecular analyses was subsequently used in the present study.

3.1 qPCR

qPCR was performed in a 96-well plate format using the Sso Advanced Universal qPCR SYBR Green Supermix (2×, Bio-Rad). Each reaction was prepared in a final volume of 10 µL.The reaction mixture per well consisted of 5.0 µL of 2× SYBR Green Supermix, 0.3 µL of forward primer 331F (10 µM, final concentration 300 nM), 0.3 µL of reverse primer 797R (10 µM, final concentration 300 nM), 1 µL of template

DNA and 3.4 µL of nuclease-free water. Each patient sample (n = 21) was pipetted into three separate wells and analyzed in technical triplicate. In addition, 7 standard dilution series and control reactions were included in each run, resulting in a total of 106 reactions. The standard dilution series consisted of *Escherichia coli* DNA (10^{-3} to 10^{-10}) and was prepared in technical triplicate to generate a calibration curve. Four non-target controls (NTCs) containing nuclease-free water were included in triplicates to monitor potential contamination. A positive control consisting of fecal DNA was included in technical triplicate to verify successful amplification. qPCR was performed on a Bio-Rad CFX96 real-time PCR system using an annealing temperature of 54 °C. Cq-values were obtained using the instruments internal software and averaged across technical triplicates prior to downstream analysis. The standard curve is provided in Figure 5.

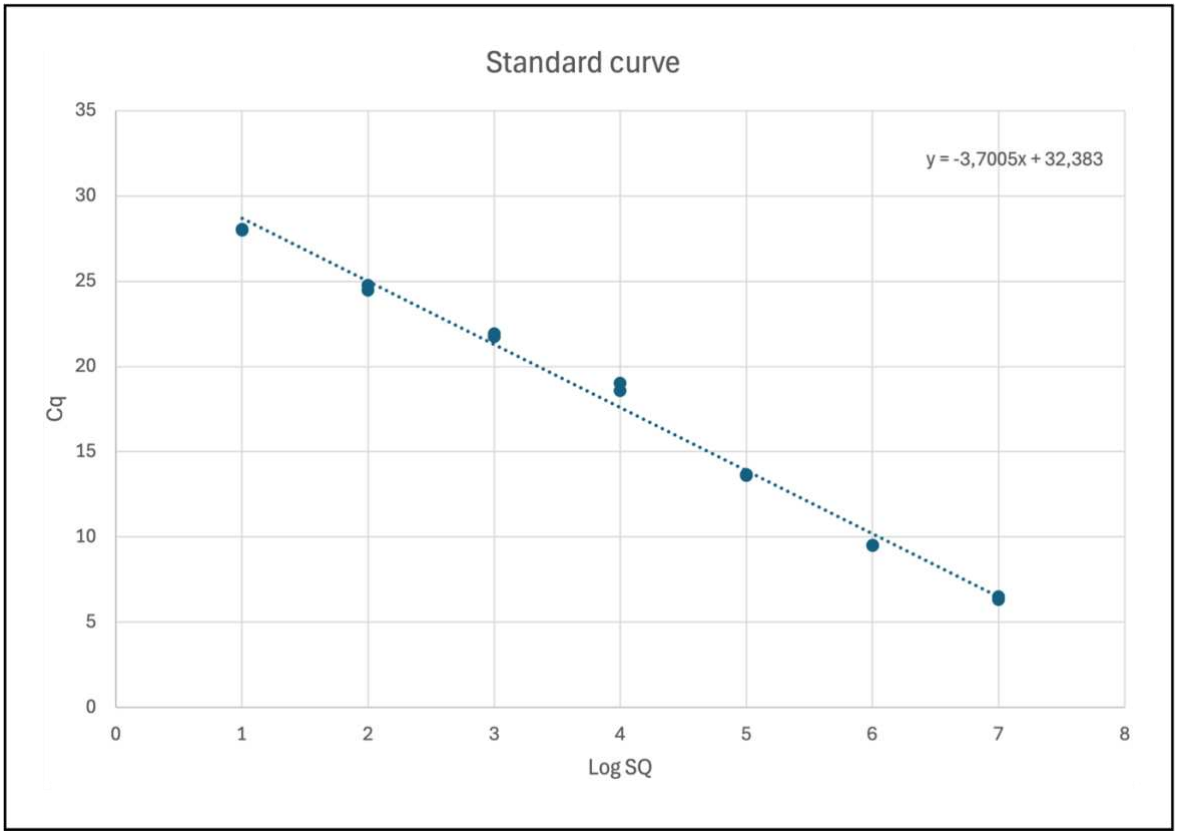

Figure 5: Standard curve (qPCR)

3.2 ddPCR

Droplet digital PCRs were performed in a reaction volume of 20 µl, containing 10 µl ddPCR Supermix for Probes (No dUTP) (Bio-Rad, United States), 1 µl forward and reverse primer (20 µM each), 1 µl probe (5 µM) and up to 8 µl template. Droplets were generated via a QX200 Droplet Generator (BioRad, United States). The sequences of the 16S targeting primer and probe set were as follows: forward primer (BACT1369F), 5'-CGGTGAATACGTTCYCGG-3'; reverse primer (PROK1492R), 5'-GGWTACCTTGTTACGACTT-3'; and probe (TM1389F), 5'-FAM-CTTGTACACACCGCCCGTC-BHQ1 (108). Cycling conditions included preheating at 95 °C for 10 min followed by 40 cycles of denaturation at 94 °C for 30 s, annealing at 55 °C for 60 s and final heating at 98 °C for 10 min. Following amplification, the PCR plate was transferred to a QX200 Droplet Reader (BioRad, United States). Generated fluorescence amplitude data was obtained via the QuantaSoft software (BioRad, United States). The corresponding amplitude threshold was set manually at 2800 for all performed measurements. The ZymoBIOMICS Microbial Community DNA Standard (Zymo Research, United States) was used to calculate the measured fluorescence concentrations with corresponding 16S copies and the overall number of bacteria present per 20 µl ddPCR reaction mix (Figure 6).

The following formula was utilized to calculate the 16S copy numbers and number of bacteria per µl ZymoBIOMICS Microbial Community DNA Standard:

16S copy number = total genomic DNA (g) × unit conversion constant (bp/g)[1] / genome size (bp) × 16S copy number per genome

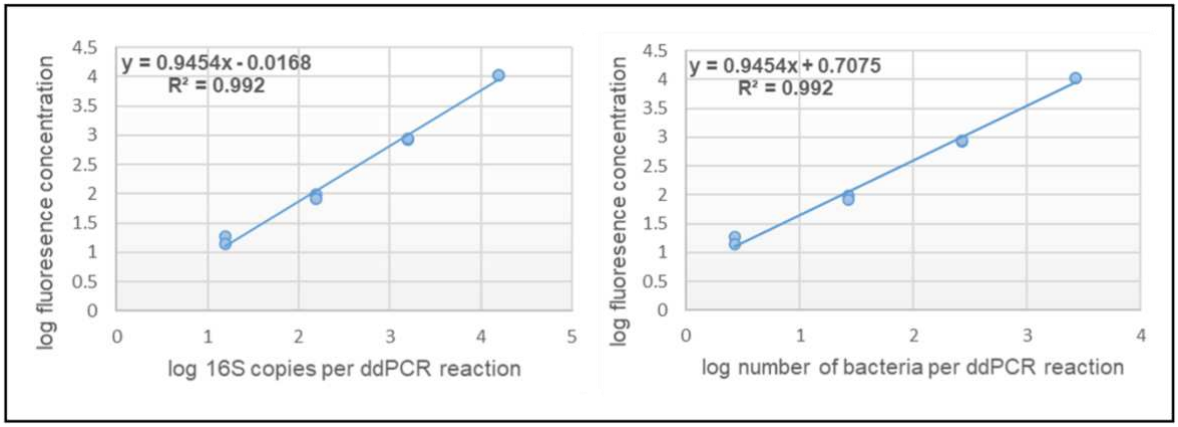

Figure 6: Correlation between fluorescence (arbitrary units) and 16S copies (left) and the number of bacteria (right) per ddPCR reaction mix. Dilutions of the standard were measured in duplicates.

[1] DNA unit conversion constant (ng/bp) = 1.079 x 10^{-12}

3.3 Histological scoring

Necrosis, mucin content and inflammatory infiltration were assessed semi-quantitatively on hematoxylin–eosin–stained sections, with all percentages estimated relative to the total tumor area. Inflammation was defined as the presence of tumor-infiltrating inflammatory cells. These percentage values were used for statistical analyses.

3.4 Statistical analysis

Statistical analyses and figures were generated using GraphPad Prism (version 10.6.1). Continuous variables were summarized using descriptive statistics (mean, standard deviation, median, interquartile range, minimum and maximum). Normality testing using the Shapiro–Wilk test was conducted when sample sizes were greater than 10. For smaller sample sizes, normality testing was not considered informative and non-parametric methods were applied. Associations between tumor group and mutation status were analyzed using Fisher's exact test due to the small sample size and low expected cell counts. To compare intratumoral bacterial abundance between primary colorectal carcinoma, primary lung cancer and lung metastasis samples, log10-transformed 16S copy numbers were analyzed for both qPCR and ddPCR using the Kruskal–Wallis test followed by Dunn's multiple comparisons test to account for multiple testing. To assess the association between qPCR and ddPCR measurements of bacterial load, correlation analysis was performed. Due to the small cohort size, formal testing for normality using the Shapiro–Wilk test was not considered informative. Therefore, Spearman's rank correlation was applied. To assess potential associations between intratumoral bacterial load and histopathological features (necrosis, mucin content and inflammation), correlation analyses were performed. Due to the small cohort size for correlations between qPCR bacterial load and histological parameters, the Shapiro-Wilk test for normality was not considered informative. Consequently, all correlations between qPCR bacterial load and histopathological variables were assessed using Spearman's rank correlation. For ddPCR-based analyses, bacterial load and histopathological percentage values showed non-normal distributions. Therefore, Spearman's rank correlation was also applied. To assess whether intratumoral bacterial abundance was associated with genetic alterations, mutation status of *KRAS*, *TP53* and

PIK3CA was compared with qPCR and ddPCR 16S copy numbers (log10-transformed). Since not all genes were assessed in every case, sample sizes varied across analyses. For ddPCR-based analyses, bacterial load values within at least one of the compared groups (mutated or wild-type) deviated from normality. For qPCR-based analyses, group sizes were too small to reliably assess normality assumptions. Therefore, non-parametric two-tailed, exact Mann–Whitney U tests were used for all comparisons between mutated and wild-type samples. A two-tailed p-value < 0.05 was considered statistically significant. Due to missing values, sample sizes varied between analyses.

4. Results

4.1 Study cohort

All 21 samples were archived specimens obtained from surgical resections performed between 2014 and 2022. The study population comprised 11 male and 10 female patients, with a median age of 70 years. The cohort included 7 primary colorectal adenocarcinomas, 7 primary lung adenocarcinomas and 7 lung metastases of colorectal adenocarcinomas. TNM staging data were available for all primary tumors, covering T stages from pT1b to pT4b and N stages from pN0 to pN2b. Histological grades ranged from G2 to G3. Tumor size (median 26.5 mm, range 8–75 mm), tumor cell content (median 60 %, range 30–80 %) and DNA concentration (median 215 ng/µL, range 78–400 ng/µL) differed across samples. The clinicopathological characteristics are summarized in Table 1. Individual sample characteristics per case are shown in detail in Supplementary Table S1a and S1b.

Among the primary colorectal cancer samples, 5 tumors were located in the right colon and 2 in the left colon. Among the 7 primary lung cancer samples, tumor localization was distributed as follows: 4 tumors in the left upper lobe (LUL), 1 in the left lower lobe (LLL), 1 in the right upper lobe (RUL) and 1 in the right lower lobe (RLL). Among the 7 lung metastases, 5 originated from left-sided colorectal primaries, 1 from a right-sided colorectal primary and in 1 case the primary tumor location was not recorded. Metastatic lung lesions were located in the left upper lobe in 2 cases, left lower lobe in 1 case, right upper lobe in 1 case, right lower lobe in 1

case and in 2 cases were documented as right lung without further lobar specification.

Table 1. Cohort characteristics

Characteristics	Value
Number of patients	21
Sex, n (%)	
Male	11 (52.4%)
Female	10 (47.6%)
Median age, years (range)	70 (49–81)
Tumor entity, n	
Primary colorectal adenocarcinoma	7
Primary lung adenocarcinoma	7
Lung metastasis of colorectal adenocarcinoma	7
TNM stage (primary tumors only)	
T stage	pT1b–pT4b
N stage	pN0–pN2b
Histological grade	G2–G3
Median maximum tumor diameter, mm (range)	26.5 (8–75)
Median tumor cell content, % (range)	60 (30–80)
Median DNA concentration (PicoGreen), ng/µL (range)	215 (78–400)

There were *KRAS* mutations in 11 of 21 samples (52.4%), while 10 samples (47.6%) were *KRAS* wild-type. *TP53* mutations were detected in 11 of 21 samples (52.4%), with the remaining 10 samples showing no *TP53* alteration. Less frequent mutations were observed in *PIK3CA* (5 of 21 samples, 23.8%). A broad panel of cancer-related gene mutations were analyzed, but mutations in most genes were generally rare. For example, one gene fusion event (*EML4::ALK*) was identified in on primary lung adenocarcinoma (case 8). For lung metastasis samples obtained between 2014 and 2017, molecular analysis was limited to selected genes according to the diagnostic standards at that time. As a result, mutation data for additional genes were not available for these cases. In later samples, broader gene panels were analyzed using next-generation sequencing (NGS). A summary of the identified molecular

alterations is provided in Table 2. Detailed mutation counts for all analyzed genes are shown in Supplementary Table S2.

Table 2. Mutation status

Gene	Mutated, n (%)	Wild-type, n (%)	NA, n (%)
KRAS	11 (52.4%)	10 (47.6%)	0 (0%)
TP53	11 (52.4%)	10 (47.6%)	0 (0%)
PIK3CA	5 (23.8%)	13 (61.9%)	3 (14.3%)
EGFR	1 (4.8%)	17 (81.0%)	3 (14.3%)

Mutation status was recorded as mutated, wildtype, or not assessed (NA).
Other gene mutations analyzed include the following genes: BRAF, APC, SMAD4, FBXW7, CTNNB1, NRAS, HRAS, ERBB2, ERBB4, PTEN, ALK, MAP2K1, FGFR2, FGFR3, KEAP1, STK11 and CDKN2A. Detailed mutation counts per gene are provided in Supplementary Table S1.

Mutation frequencies did not differ significantly among primary CRC, primary lung cancer and lung metastasis samples. No significant association between tumor group and KRAS mutation status was observed (Fisher's exact test, p = 0.42). Likewise, TP53 mutation frequency did not differ significantly between groups (Fisher's exact test, p = 0.42). Similarly, no significant association was found for PIK3CA mutation status (Fisher's exact test, p = 0.79). *KRAS* and *PIK3CA* mutation status across tumor groups is shown in Figure 7. *TP53* mutation frequencies demonstrated an identical distribution and statistical result as *KRAS* mutations and are therefore not shown separately, although this reflects only an identical number of mutated and non-mutated cases rather than mutations occurring in the same samples

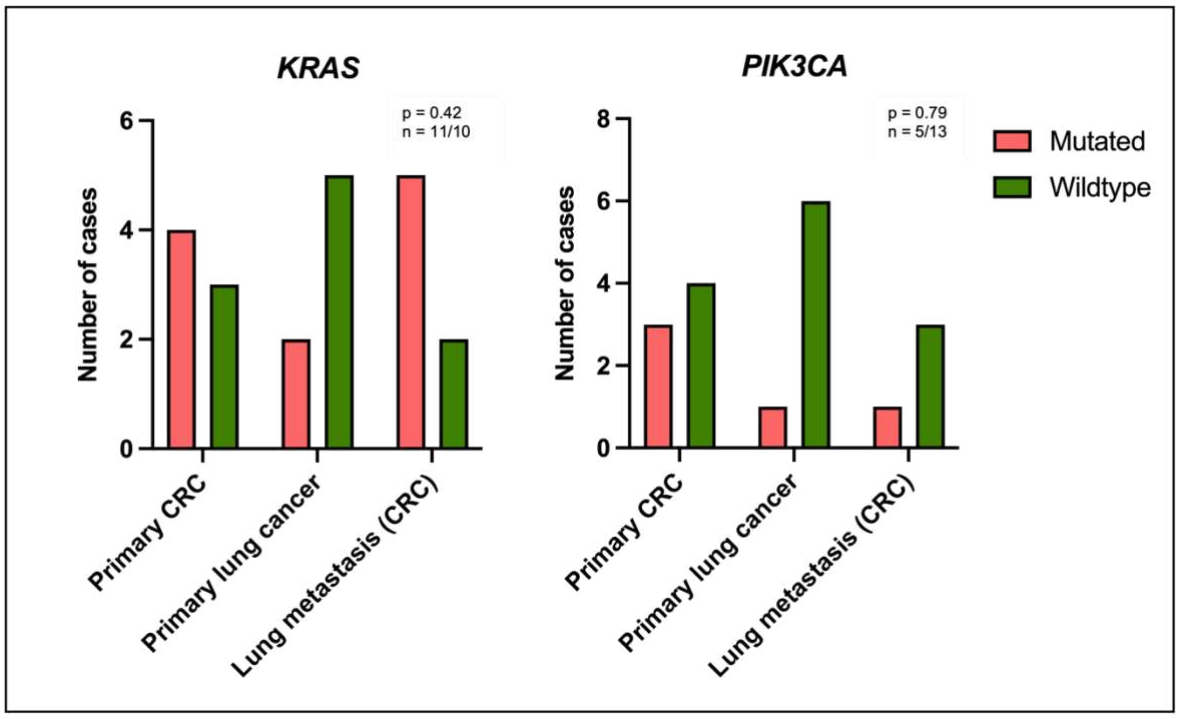

Figure 7: Association between mutation status and tumor group.

4.2 qPCR results

Samples showing large variability (SD Cq > 0.5) among all three technical replicates were considered unreliable. Based on this criterion, samples 2, 8, 9, 18 and 19 were excluded due to excessive dispersion among triplicate Cq values. In addition, samples 6, 11, 13, 16, 17 and 21 showed insufficient microbial DNA concentration, resulting in undetectable or non-reproducible amplification signals and were therefore excluded. NTCs yielded Cq values between 31.46 and 37.22. To account for background signal, the lowest negative control Cq value (31.46) was defined as a threshold. Samples with Cq values exceeding this threshold were considered indistinguishable from background. After applying all quality control criteria, 10 of 21 samples remained eligible for qPCR-based analysis (samples 1, 3, 4, 5, 7, 10, 12, 14, 15 and 20). For the remaining samples, starting quantity (SQ) values derived from the standard curve were used as a quantitative proxy for bacterial load (higher SQ indicates higher microbial DNA abundance). Mean SQ values were calculated from technically consistent triplicates and log10-transformed to reduce right-skewness and stabilize variance and can be referred to as bacterial 16S copy numbers, as 1 µL of template DNA was used per reaction, making the estimated starting quantity directly interpretable as copies per reaction.

In descriptive analysis, primary colorectal carcinoma (CRC) samples showed the highest copy numbers (mean 2.61, median 2.65, n = 5), whereas primary lung cancer samples exhibited the lowest copy numbers (mean 1.25, median 1.14, n = 3). Lung metastases of CRC demonstrated intermediate copy numbers (mean 2.21, median 2.21, n = 2). Descriptive statistics of log10-transformed 16S copy numbers are summarized in Table 3.

Table 3. log10 16S copy numbers (qPCR)

	Primary CRC	Primary lung cancer	Lung metastasis (CRC)
Number of values	5	3	2
Minimum	2.03	1.14	1.55
25% Percentile	2.21	1.14	1.55
Median	2.65	1.14	2.21
75% Percentile	2.99	1.47	2.86
Maximum	3.16	1.47	2.86
Range	1.13	0.33	1.31
Mean	2.61	1.25	2.21
Std. Deviation	0.429	0.191	0.926
Std. Error of Mean	0.192	0.11	0.655

Normality was assessed using the Shapiro–Wilk test. Primary CRC samples did not deviate from normal distribution (W = 0.9964, p = 0.9967), whereas primary lung cancer samples failed the normality test (W = 0.7500). Normality testing was not performed for lung metastasis samples due to the very small sample size (n = 2). Given the small and uneven group sizes, non-parametric testing was applied for group comparisons.

Copy numbers differed significantly among primary CRC, primary lung cancer and lung metastasis samples (Kruskal–Wallis test, $H = 5.84$, $p = 0.032$, $n = 10$). However, post hoc analysis using Dunn's multiple comparisons test did not reveal statistically significant pairwise differences between any of the groups. Comparisons between primary CRC and primary lung cancer (adjusted $p = 0.055$), primary CRC and lung metastasis samples (adjusted $p > 0.999$), and primary lung cancer and lung metastasis samples (adjusted $p = 0.31$) were all non-significant after correction for multiple testing. Group comparisons are shown in Figure 5. Detailed qPCR results are provided in Supplementary Table S4.

4.3 ddPCR results

Mean ddPCR 16S copy numbers were log10-transformed to reduce right-skewness and stabilize variance, thereby improving comparability between samples. In descriptive analysis, primary colorectal carcinoma (CRC) samples showed the highest copy numbers (mean 3.86, median 3.41, n = 7), compared with primary lung carcinoma samples, which exhibited the lowest values (mean 1.85, median 1.83, n = 7). Lung metastases of CRC demonstrated intermediate copy numbers (mean 2.51, median 2.21, n = 7). Overall, these findings are consistent with the qPCR results. Descriptive statistics are summarized in Table 4.

Table 4. log10 16S copy numbers (ddPCR)			
	Primary CRC	**Primary lung cancer**	**Lung metastasis (CRC)**
Number of values	7	7	7
Minimum	2.87	1.58	1.73
25% Percentile	3.12	1.69	2.01
Median	3.41	1.83	2.21
75% Percentile	4.72	1.97	2.96
Maximum	5.15	2.19	4.30
Range	2.28	0.605	2.57
Mean	3.86	1.85	2.51
Std. Deviation	0.891	0.198	0.878
Std. Error of Mean	0.337	0.0748	0.332

Normality was assessed using the Shapiro–Wilk test. Primary CRC ($W = 0.8937$, $p = 0.2948$) and primary lung cancer samples ($W = 0.9849$, $p = 0.9797$) did not deviate from normal distribution. In contrast, lung metastasis samples showed a significant deviation from normality ($W = 0.7963$, $p = 0.0376$). As the assumption of normal distribution was violated in at least one group, non-parametric testing was applied for group comparisons.

Copy numbers differed significantly among primary CRC, primary lung cancer and lung metastasis samples (Kruskal–Wallis test, $H = 13.74$, $p < 0.0001$, $n = 21$). Post hoc analysis using Dunn's multiple comparisons test revealed significantly higher bacterial load in primary CRC compared to primary lung cancer (adjusted $p = 0.0006$). No significant differences were observed between primary CRC and lung metastasis samples (adjusted $p = 0.14$) nor between primary lung cancer and lung metastasis samples (adjusted $p = 0.26$).

Copy numbers (log10-transformed) with median and interquartile range per group are shown in Figure 8. Individual ddPCR copies per sample are provided in the Supplementary Table S5.

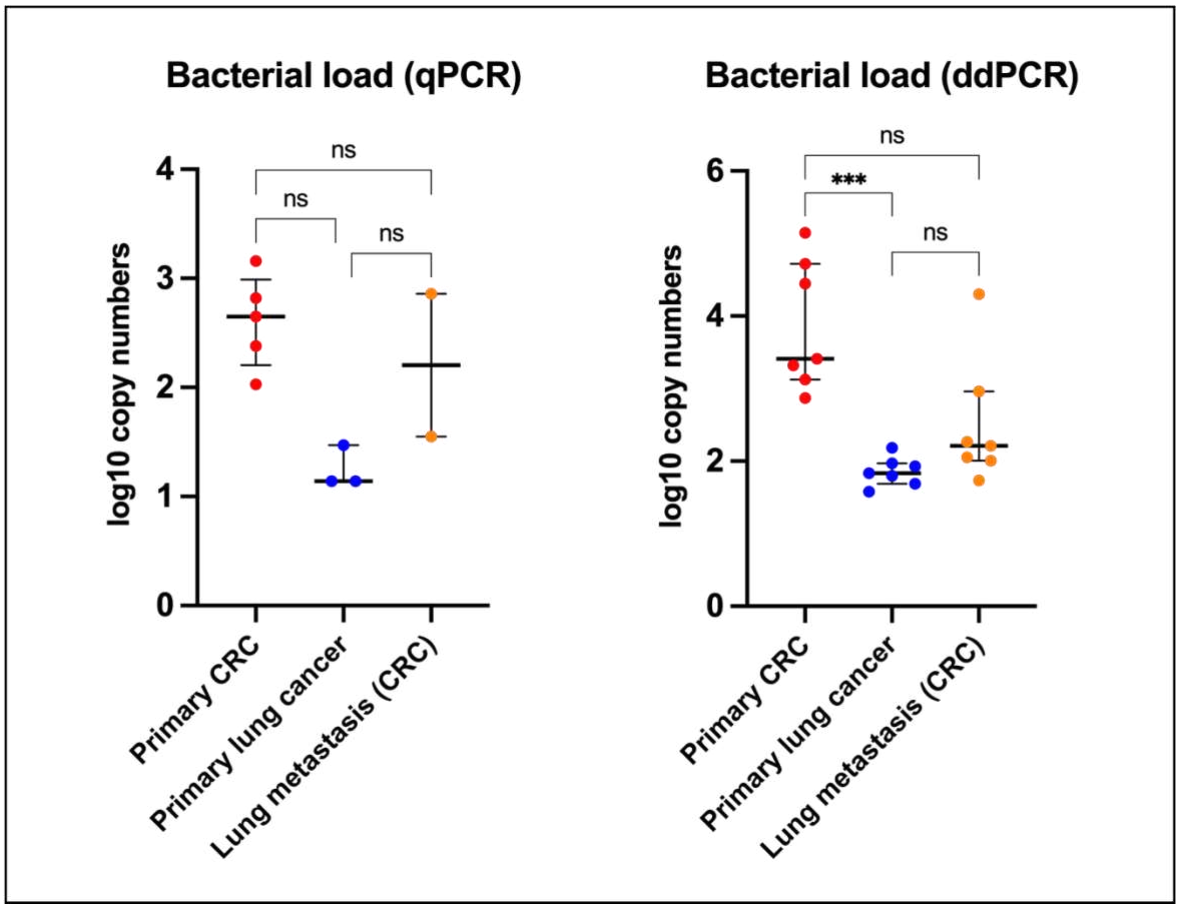

*Figure 8: 16S copy numbers measured by qPCR (left) and ddPCR (right) across sample groups. Data are shown as individual values with medians and IQR. ***p < 0.001. ns = not significant.*

4.4 Histological scoring of tumor necrosis, mucin content & inflammatory infiltrate

4.4.1 Necrosis

In descriptive analysis, lung metastases of CRC showed the highest necrosis percentages (mean 45%, median 40%, n = 7), compared with primary colorectal carcinoma (CRC) samples (mean 12.3%, median 10%, n = 7) and primary lung carcinoma samples, which exhibited the lowest values (mean 12.3%, median 10%, n = 7). Descriptive statistics are summarized in Table 5. An example for a necrotic tumor is provided in Figure 9 (A-C).

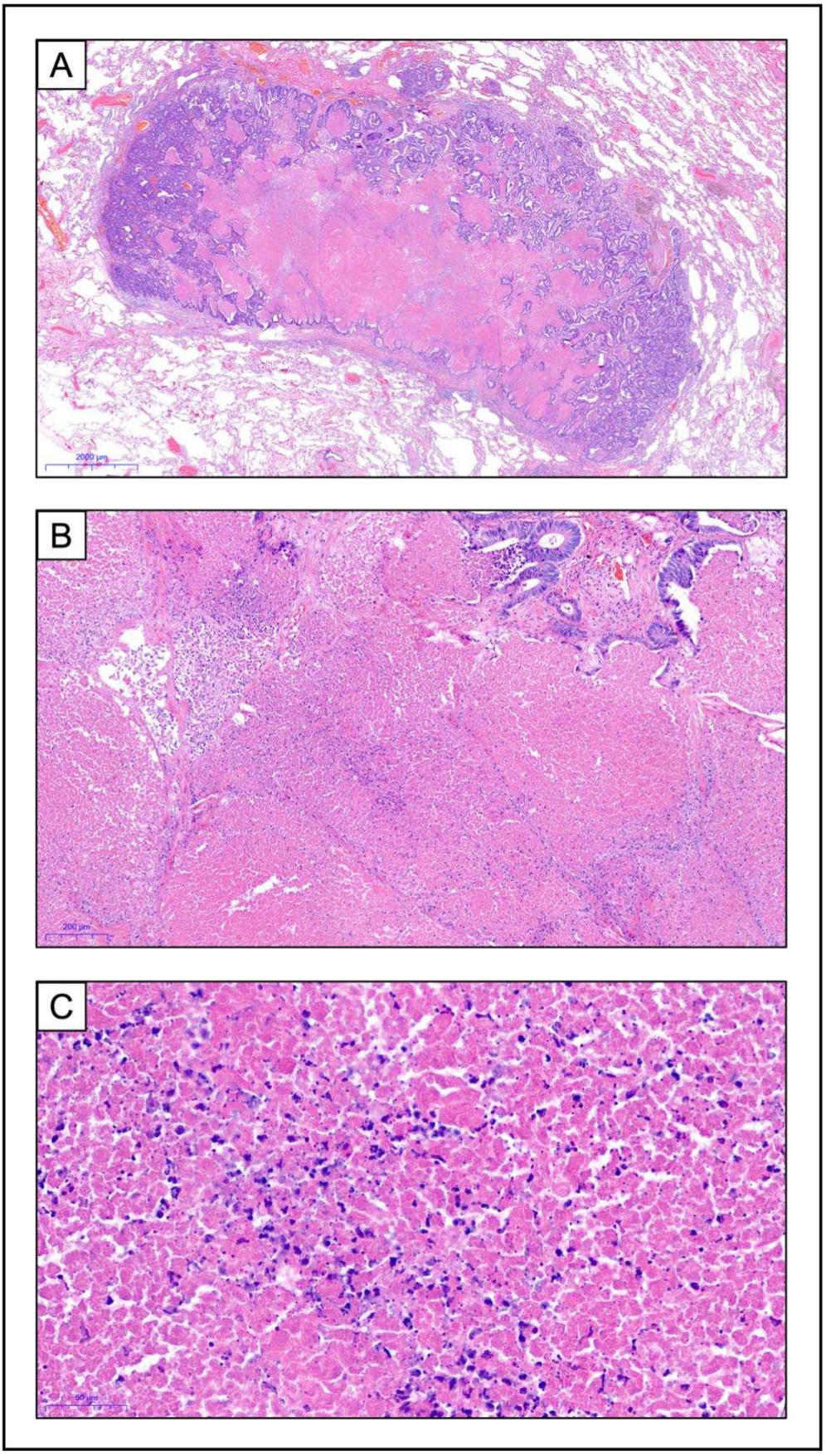

Figure 9: Histological H&E-stained section of necrosis within a lung metastasis at increasing magnification. (A) Low-power overview. (B) Intermediate magnification highlighting the necrotic area. (C) High-power detail view of the necrotic tissue. Scale bar shown in the lower left corner.

Normality was assessed using the Shapiro–Wilk test. Primary CRC ($W = 0.8996$, $p = 0.3286$) and lung metastasis samples ($W = 0.9308$, $p = 0.5574$) did not deviate from normal distribution. In contrast, primary lung cancer samples showed a significant deviation from normality ($W = 0.6761$, $p = 0.0020$). As the assumption of normal distribution was violated in at least one group, non-parametric testing was applied for subsequent group comparisons.

Necrosis percentages differed significantly among primary CRC, primary lung cancer and lung metastasis samples (Kruskal–Wallis test, $H = 8.93$, $p = 0.0066$, $n = 21$). Post hoc analysis using Dunn's multiple comparisons test revealed significantly higher necrosis levels in lung metastasis samples compared to primary CRC (adjusted $p = 0.0448$) and primary lung cancer samples (adjusted $p = 0.0198$). No significant difference was observed between primary CRC and primary lung cancer samples (adjusted $p > 0.9999$) (Figure 10).

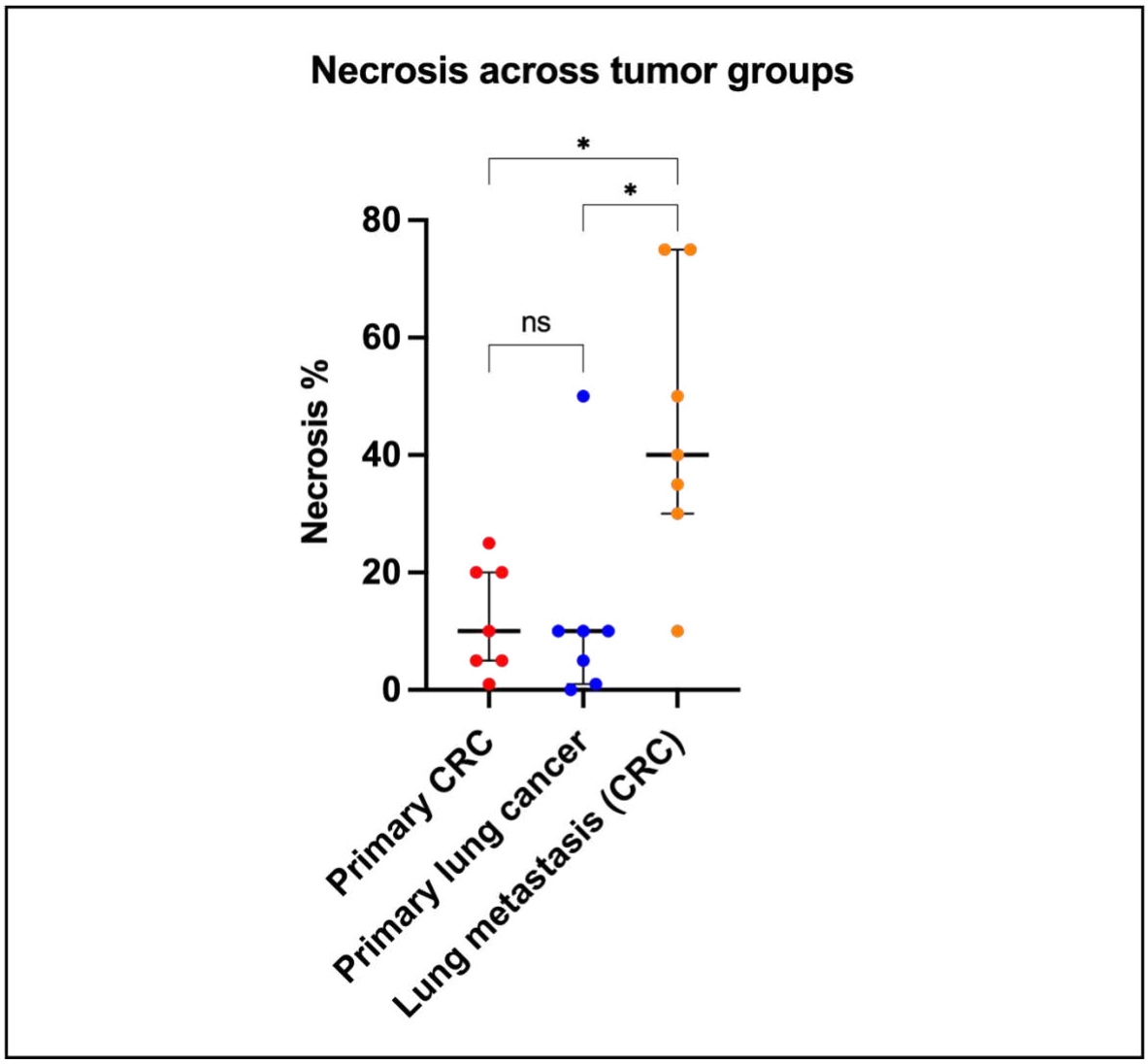

*Figure 10: Necrosis percentage relative to the tumor area across tumor groups. Data are shown as individual values with medians and IQR. *p < 0.05. ns = not significant.*

4.4.2 Mucine

In descriptive analysis, primary lung carcinoma samples showed the highest mucin percentages (mean 10.7%, median 5%, n = 7), compared with lung metastases of CRC (mean 6.14%, median 1%, n = 7) and primary colorectal carcinoma (CRC) samples, which exhibited comparable but slightly lower values (mean 5.29%, median 5%, n = 7). Descriptive statistics are summarized in Table 5. An example for a mucinous tumor is provided in Figure 11 (A-C).

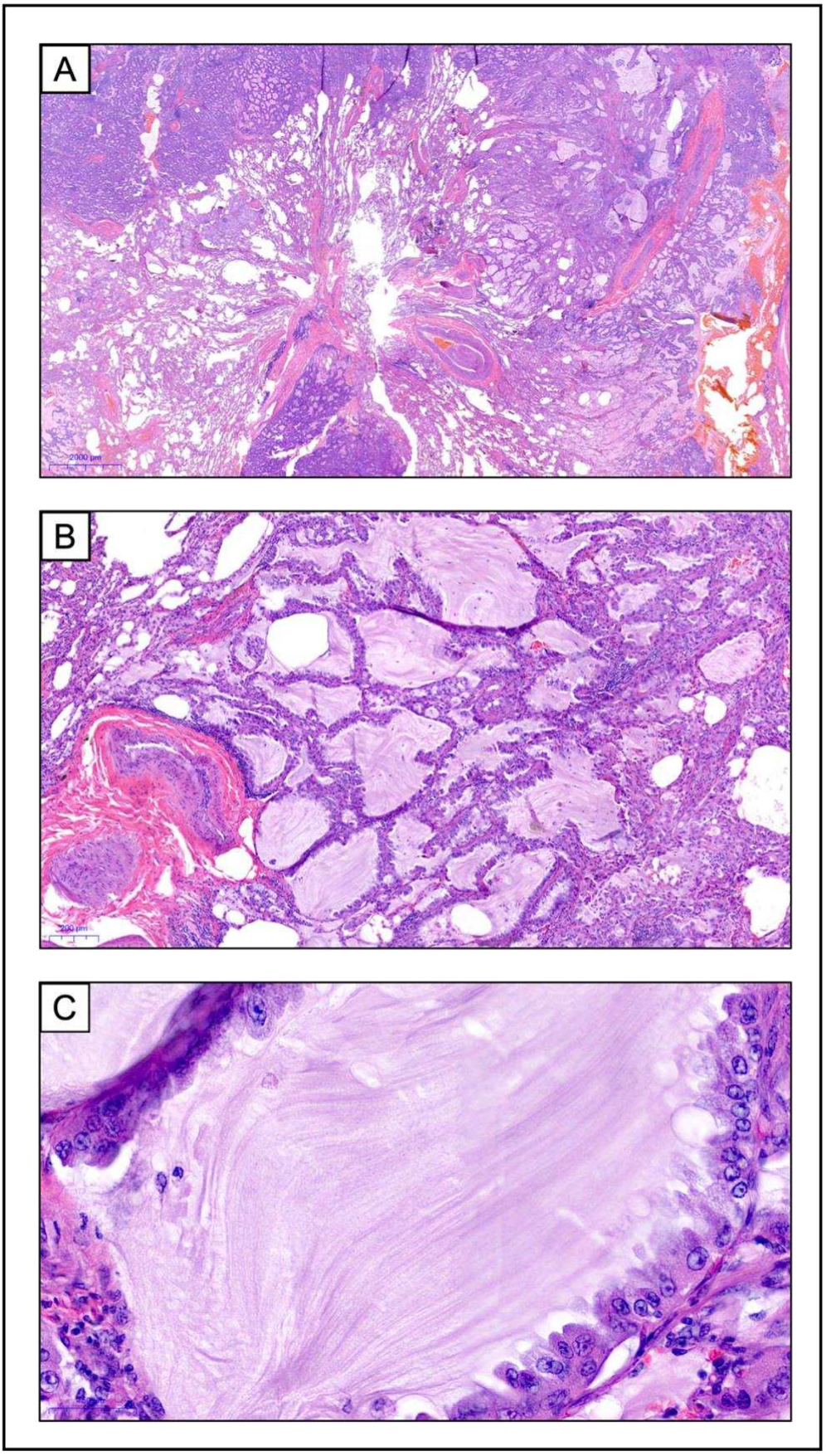

Figure 11: Histological H&E-stained section of mucin within a primary lung tumor at increasing magnification. (A) Low-power overview. (B) Intermediate magnification with mucinous areas. (C) High-power detail view of intratumoral mucin. Scale bar shown in the lower left corner.

Normality was assessed using the Shapiro–Wilk test. All three groups deviated significantly from normal distribution: primary CRC (W = 0.7204, p = 0.0062), primary lung cancer (W = 0.6877, p = 0.0027), and lung metastasis samples (W = 0.7283, p = 0.0075). Therefore, non-parametric tests were used for group comparisons. Mucin percentages did not differ significantly among primary CRC, primary lung cancer and lung metastasis samples (Kruskal–Wallis test, H = 1.51, p = 0.4958, n = 21). Post hoc analysis using Dunn's multiple comparisons test confirmed the absence of significant differences between any of the groups (primary CRC vs. primary lung cancer: adjusted p = 0.8631, primary CRC vs. lung metastasis: adjusted p > 0.9999, primary lung cancer vs. lung metastasis: adjusted p = 0.8631).

4.4.3 Inflammation

In descriptive analysis, primary lung carcinoma samples showed the highest inflammation percentages (mean 16.4%, median 10%, n = 7), compared with lung metastases of CRC (mean 10.7%, median 10%, n = 7) and primary colorectal carcinoma (CRC) samples, which exhibited the lowest values (mean 8.57%, median 5%, n = 7). Descriptive statistics are summarized in Table 5. An example for a tumor with inflammatory infiltration is provided in Figure 12 (A-C).

Normality was assessed using the Shapiro–Wilk test. Primary CRC (W = 0.5819, p = 0.0002) and primary lung cancer samples (W = 0.7499, p = 0.0127) showed significant deviation from normal distribution, whereas lung metastasis samples did not deviate significantly from normality (W = 0.8163, p = 0.0591). As the assumption of normal distribution was violated in at least one group, non-parametric tests were applied for subsequent group comparisons.

Inflammation percentages did not differ significantly among primary CRC, primary lung cancer and lung metastasis samples (Kruskal–Wallis test, H = 3.61, p = 0.1674, n = 21). Post hoc analysis using Dunn's multiple comparisons test confirmed the absence of significant differences between any of the groups (primary CRC vs. primary lung cancer: adjusted p = 0.1723, primary CRC vs. lung metastasis: adjusted p > 0.9999, primary lung cancer vs. lung metastasis: adjusted p = 0.9748). Detailed histological scoring is provided in Supplementary Table S6.

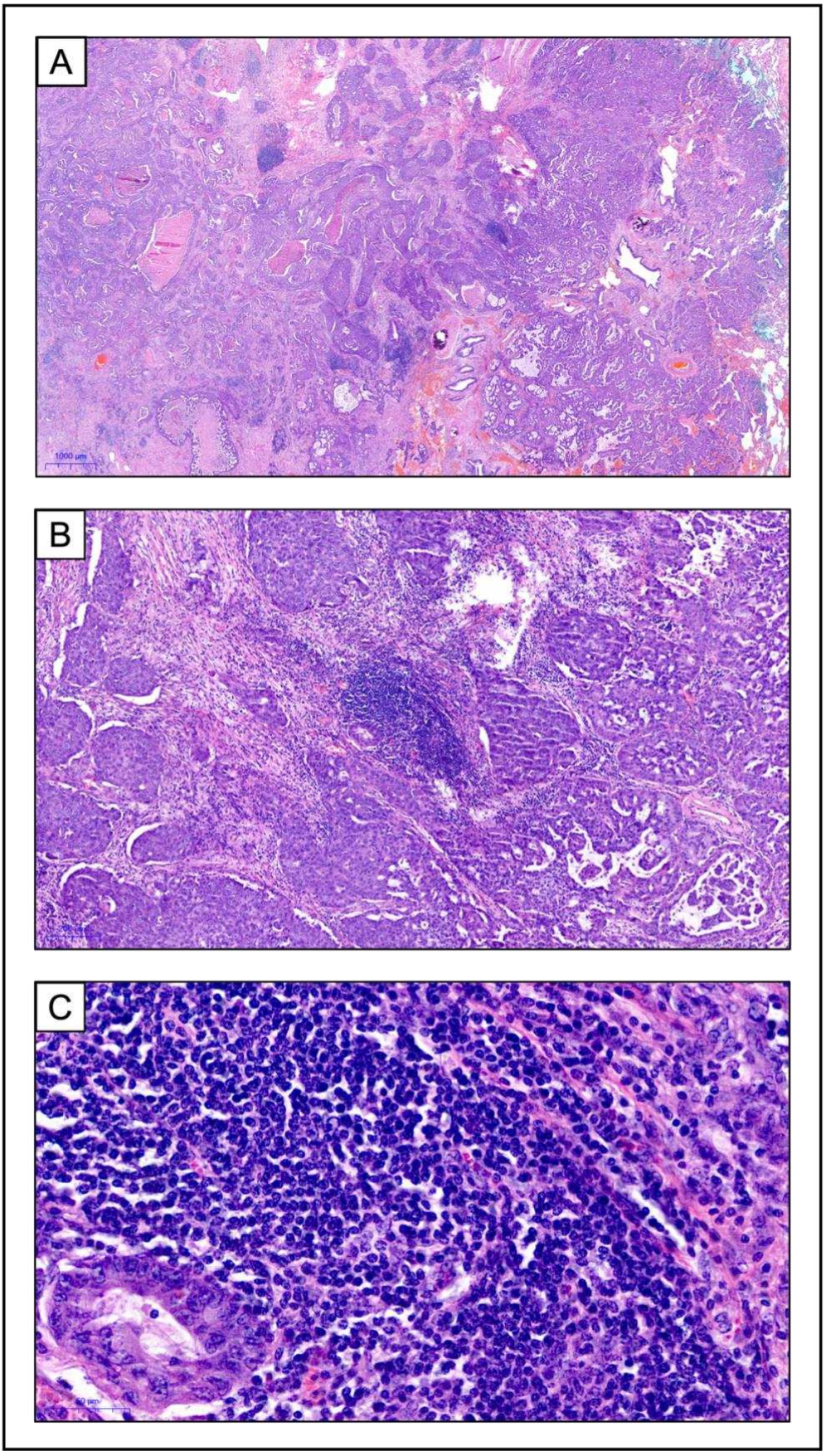

Figure 12: Histological H&E-stained section of lymphocytic inflammation within a primary lung tumor at increasing magnification. (A) Low-power overview. (B) Intermediate magnification highlighting the inflammatory infiltrate. (C) High-power detail view of tumor-infiltrating lymphocytes. Scale bar shown in the lower left corner.

Table 5. Descriptive statistics of histological scoring			
	Primary CRC	**Primary lung cancer**	**Lung metastasis (CRC)**
Necrosis (%)			
Number of values	7	7	7
Minimum	1	0	10
25% Percentile	5	1	30
Median	10	10	40
75% Percentile	20	10	75
Maximum	25	50	75
Range	24	50	65
Mean	12.3	12.3	45
Std. Deviation	9.3	17.2	23.8
Std. Error of Mean	3.52	6.49	9
Mucine (%)			
Number of values	7	7	7
Minimum	0	0	0
25% Percentile	1	5	1
Median	5	5	1
75% Percentile	5	10	10
Maximum	20	40	25
Range	20	40	25
Mean	5.29	10.7	6.14
Std. Deviation	6.85	13.4	9.03
Std. Error of Mean	2.59	5.05	3.41
Inflammation (%)			
Number of values	7	7	7
Minimum	5	5	5
25% Percentile	5	10	5
Median	5	10	10
75% Percentile	10	30	15
Maximum	25	40	25
Range	20	35	20
Mean	8.57	16.4	10.7
Std. Deviation	7.48	13.1	7.32
Std. Error of Mean	2.83	4.97	2.77

4.5 Bacterial load in qPCR and ddPCR

Due to the small sample size (n = 10), formal testing for normality was not considered informative. Therefore, correlation analysis was performed using Spearman's rank correlation. A strong positive correlation was observed between qPCR and ddPCR measured log10-transformed 16S copy numbers (Spearman r = 0.90, p = 0.0009, n = 10) (Figure 13).

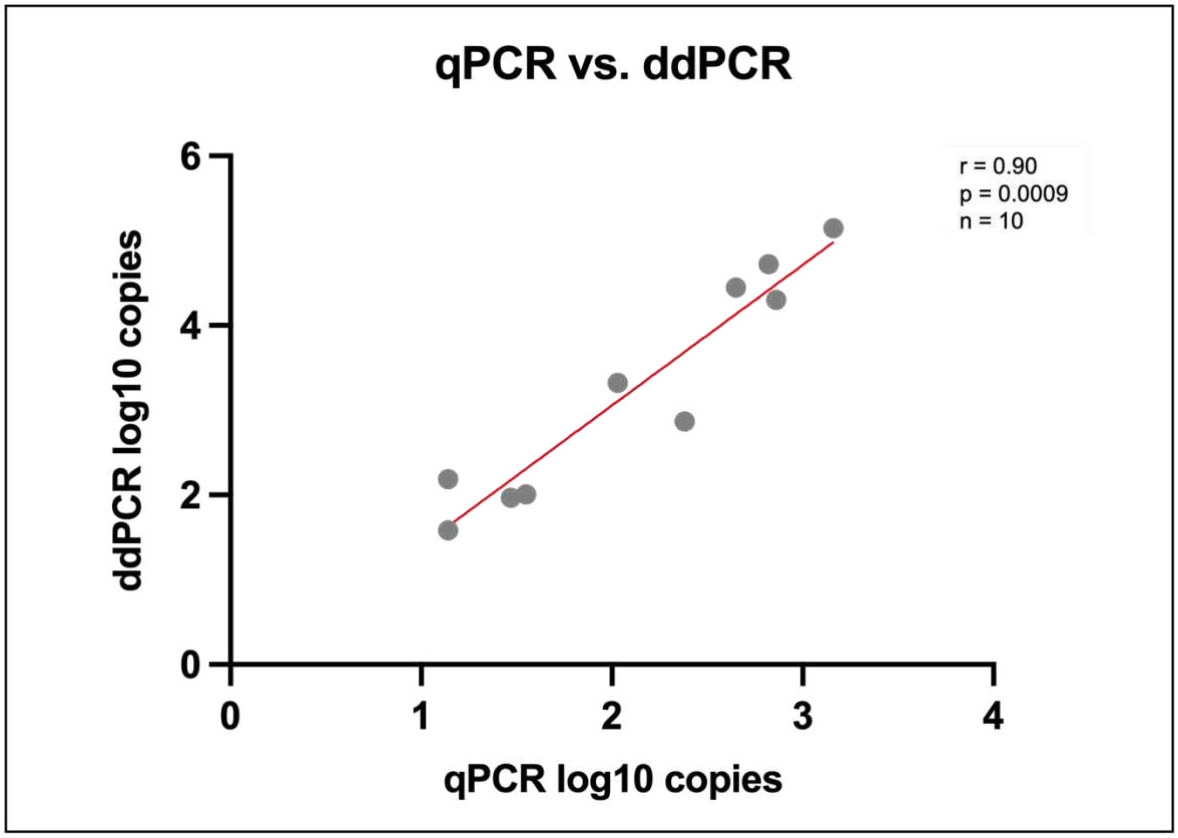

Figure 13: Spearman's rank correlation between 16S copy numbers of qPCR and ddPCR.

4.6 Bacterial load and histopathological parameters

Given the small sample size (n = 10), formal assessment of normality was considered unreliable for qPCR-measured copy numbers. Therefore, correlations were evaluated using Spearman's rank correlation. No significant correlations were observed between mean qPCR bacterial load and histopathological parameters. Specifically, bacterial load did not correlate with tumor necrosis (Spearman r = 0.33, p = 0.35, n = 10), mucin content (Spearman r = −0.06, p = 0.87, n = 10), or inflammation (Spearman r = −0.38, p = 0.27, n = 10).

The Shapiro–Wilk test demonstrated significant deviation from normality for ddPCR-measured bacterial load (W = 0.8571, p = 0.0056). Consequently, the Spearman‘s rank correlation was used. No significant correlations were observed between ddPCR measured bacterial load and necrosis (Spearman r = 0.11, 95% CI −0.35 to 0.53, p = 0.62, n = 21) or mucin content (Spearman r = −0.37, 95% CI −0.70 to 0.09, p = 0.10, n = 21). In contrast, ddPCR measured bacterial load showed a significant negative correlation with inflammation (Spearman r = −0.65, 95% CI −0.85 to −0.29, p = 0.0015, n = 21) (Figure 14).

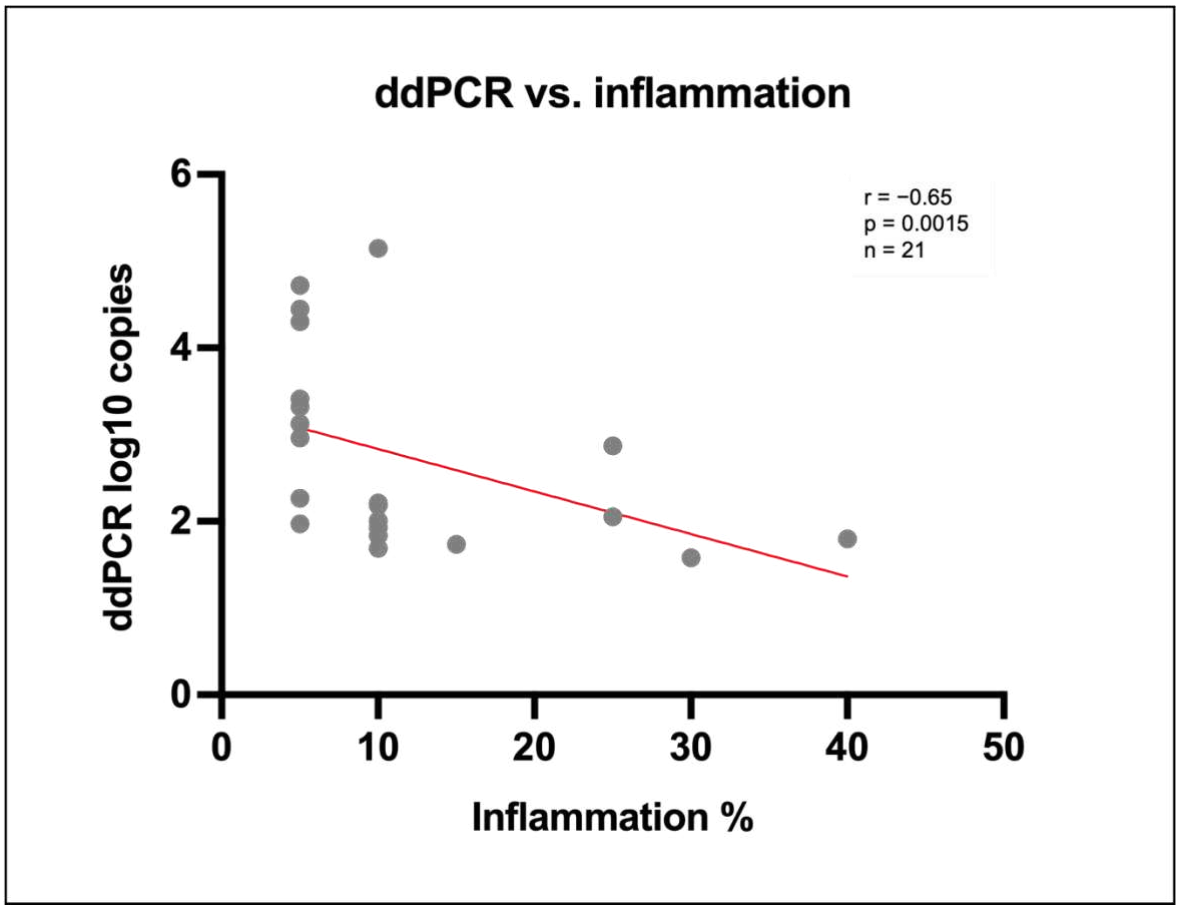

Figure 14: Spearman’s rank correlation between bacterial load (ddPCR) and inflammation percentage relative to the tumor area.

4.7 Bacterial load and genomic mutations

Due to the small sample size (n = 10) for comparison of qPCR copy numbers and mutation status, normality was not assessed and non-parametric testing was applied. Bacterial load measured through qPCR did not differ significantly between mutated and wild-type tumors for any of the analyzed genes. No significant difference was observed between *KRAS*-mutated and *KRAS* wild-type samples (Mann–Whitney U = 3, p = 0.11, median 2.82 [n = 3] vs. 1.55 [n = 7]), *TP53*-mutated and *TP53* wild-type samples (U = 8, p = 0.44, median 2.21 [n = 6] vs. 1.90 [n = 4]), or *PIK3CA*-mutated and *PIK3CA* wild-type samples (U = 2, p = 0.156, median 2.84 [n = 2] vs. 1.790 [n = 8]).

Since at least one of the variables deviated from normal distribution, comparisons between ddPCR-measured bacterial load and genetic alterations were performed using the non-parametric Mann–Whitney U test. Bacterial load measured through ddPCR also did not differ significantly between *KRAS*-mutated and *KRAS* wild-type samples (Mann–Whitney U = 37, p = 0.22, median 2.96 [n = 11] vs. 2.03 [n = 10]), *TP53*-mutated and *TP53* wild-type samples (U = 43, p = 0.42, median 2.87 [n = 11] vs. 2.12 [n = 10]), or *PIK3CA*-mutated and *PIK3CA* wild-type samples (U = 18, p = 0.17, median 3.41 [n = 5] vs. 2.01 [n = 13]). Bacterial load and KRAS/TP53 mutation status are visualized in Figure 15 below.

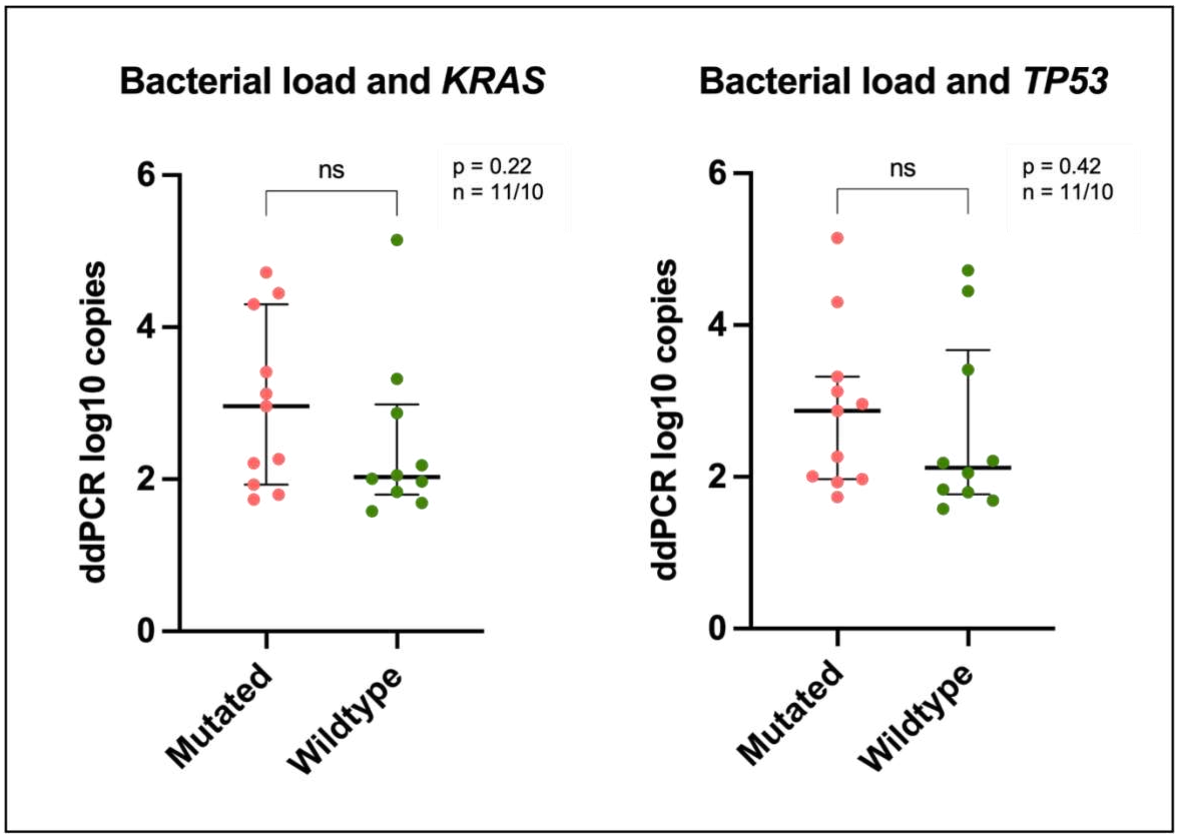

Figure 15: Bacterial load (ddPCR) by KRAS mutation status (left) and TP53 mutation status (right). Data are shown as individual values with medians and IQR. ns = not significant.

5. Discussion

Colon and lung cancer are among the leading causes of cancer-related death worldwide (1,3). To properly improve cancer care, a deep understanding of the tumor biology is needed. The TME and its associated microbiota have become increasingly important over the last decades as new technologies enabled us to understand the complex interplay between tumor cells, non-malignant cells and microbes. Although the intratumoral microbiota is still a topic that leads to a lot of controversy in the scientific community, various studies have shown that bacteria can affect tumor biology in various ways (81,102,103).

In this study, intratumoral bacterial load was quantified in a total of 21 cases of primary colorectal cancer, primary lung cancer and colorectal cancer metastases to the lung using 16S rRNA qPCR and ddPCR. In addition, semiquantitative histological scoring of necrosis, mucin content and inflammation were performed. The 16S rRNA gene copy numbers were used as a proxy for the intratumoral

bacterial load and compared with the histopathological parameters and the mutation status of *KRAS*, *TP53* and *PIK3CA*. A key finding of this study was that inflammation was the only histopathological parameter significantly associated with intratumoral bacterial load and this association was observed exclusively for ddPCR measured 16S rRNA copy numbers. Given the smaller effective sample size (n = 10) and the lower detection sensitivity of qPCR, the study may have been underpowered to detect an association between qPCR-derived bacterial load and inflammation. No significant correlations were detected between bacterial load and necrosis, mucin content or the analyzed genetic mutations.

Droplet digital PCR proved superior to qPCR for the detection and quantification of bacterial DNA in samples with low bacterial abundance. This is because ddPCR enables absolute quantification without reliance on standard curves, thereby providing improved precision and robustness in low-microbial biomass samples (93). In contrast, qPCR-based analyses were limited by lower sensitivity and by the reduced cohort size following quality control which likely contributed to the absence of significant associations for qPCR bacterial load.

Importantly, 16S rRNA gene copy numbers measured by qPCR and ddPCR showed a strong positive correlation, indicating that both methods detect comparable biological signals despite differences in sensitivity and robustness. This suggests that ddPCR does not identify a fundamentally different microbial pattern but rather provides improved detection reliability in low-biomass samples. The absence of significant associations in qPCR-based analyses is therefore most likely attributable to reduced sensitivity and smaller effective sample size.

In qPCR-based group comparison the global Kruskal–Wallis test indicated a significant difference among groups but pairwise comparisons did not remain significant after correction for multiple testing. This likely reflects limited statistical power due to the small sample size. ddPCR-based group comparisons demonstrated significantly higher intratumoral bacterial load in primary colorectal carcinomas compared to primary lung cancers. Lung metastases of colorectal origin showed intermediate bacterial levels and did not differ significantly from either primary tumor group. These findings are biologically plausible, as colorectal tumors

arise within a microbiota-rich environment, whereas primary lung tumors develop in a comparatively low-biomass tissue compartment (53,109). The intermediate bacterial load observed in lung metastases may reflect their colonic origin while also indicating potential adaptation to the pulmonary microenvironment.
In addition, necrosis differed significantly among tumor entities, with colorectal lung metastases exhibiting higher necrotic percentages compared to both primary colorectal and primary lung carcinomas. Despite this group difference, no significant association between necrosis and intratumoral bacterial load was observed. This indicates that the higher bacterial load detected in primary colorectal tumors is unlikely to be explained by differences in necrotic tissue proportions alone. Although necrotic regions may influence DNA integrity and local microenvironmental conditions, necrosis does not appear to represent a major confounding factor in the present analysis.

The observed inverse association between ddPCR bacterial load and tumor-associated inflammation is biologically plausible. Increased immune cell infiltration and inflammatory activity within the tumor microenvironment may contribute to enhanced bacterial clearance, resulting in reduced bacterial DNA content. Similar interactions between tumor-associated bacteria and immune cell infiltration have been described previously, supporting the concept that intratumoral microbiota and inflammation are closely linked (110–112). Although a significant correlation was observed, causality cannot be assumed from this analysis. It remains unclear whether inflammation actively reduces bacterial persistence or whether low bacterial abundance contributes to a more inflammatory TME as microbiota exhibiting dual roles in modulating immune and inflammatory pathways has been described in the literature (113).

Notably, inflammation scores did not differ significantly between tumor entities. This suggests that the observed differences in intratumoral bacterial load between primary colorectal and lung cancers cannot be attributed to systematic differences in inflammatory infiltration across groups. The inverse association between inflammation and bacterial load therefore appears to reflect a tumor-level relationship independent of tumor type.

No significant correlations were observed between bacterial load and necrosis or mucin content. Tumor necrosis represents areas of non-living tissue, which may limit the amount of both tumor cells and bacteria, potentially reducing detectable bacterial DNA.
Oosterlinck et al. have shown that the composition of intratumoral bacterial taxa varies depending on mucin content (114). These findings indicate that mucin may influence microbial colonization patterns and it is therefore plausible that changes in relative bacterial composition could also be accompanied by alterations in overall bacterial abundance, which were not detectable in our cohort. The semiquantitative nature of histological scoring of only one slide per tumor sample and the limited cohort size likely reduced the ability to detect subtle associations.

No significant differences in bacterial load were observed between mutated and wild-type tumors for *KRAS*, *TP53*, or *PIK3CA*. While bacterial abundance and genetic alterations are known to be associated in certain tumor entities, the inconsistent availability of molecular genetic data and the small cohort size limited the statistical power of these analyses (115–118). Consequently, potential associations between intratumoral microbiota and genetic alterations cannot be excluded and should be addressed in larger, systematically characterized cohorts.

An important strength of this study is the use of DNA extracted during routine pathological work-up, demonstrating that archival material can serve as a source for microbial detection. Importantly, DNA was obtained from serial FFPE sections directly following the histologically assessed slides. This approach minimized sampling bias related to intratumoral heterogeneity and enables a direct correlation between histological features and microbial measurements. Because DNA was derived from material generated as part of the standard diagnostic pathology workflow, this strategy could be integrated into routine pathological cancer diagnostics without additional tissue processing or sampling. As previously described, the microbiota plays a crucial role in tumor biology and cancer treatment (35, 73-82). Studies have also shown that absolute bacterial load as well as the presence of specific bacterial taxa have prognostic relevance (112,115,119,120). Determining which bacterial species are present and their relative abundances within the tumor, using complementary molecular approaches such as PCR and

NGS, may provide valuable insights for identifying individualized cancer treatment strategies.

However, several limitations of our study must be acknowledged. The overall sample size was small and qPCR analyses were further limited by failed amplifications. Furthermore, 16S rRNA gene copy numbers do not directly reflect bacterial cell numbers, as different bacterial species harbor varying numbers of 16S rRNA gene copies per genome, typically ranging from one to approximately fifteen copies (121). Therefore, bacterial load should be interpreted as a proxy for microbial abundance rather than an absolute bacterial count. Reduced amplification efficiency observed in qPCR analyses may be due to technical factors, including primer degradation over time and pipetting variability. Inaccurate calibration of pipettes can introduce systematic errors, particularly when working with low-copy-number templates. These limitations could be addressed by using fresh primers and the calibration of pipettes prior to PCR. Performing multiple independent qPCR runs and calculating mean values may further improve reproducibility and reduce measurement variability.

Further limitations concern potential extraction bias and background contamination associated with FFPE material. Formalin fixation and paraffin embedding may introduce low levels of environmental bacterial DNA. To control for this, future studies should include extraction blanks and paraffin-only controls processed in parallel with tissue samples. In addition, different extraction protocols could be compared to assess variability in bacterial recovery. The use of freshly obtained surgical tissue collected under sterile conditions could reduce contamination and improve specificity of microbial detection. However, this approach would not allow the use of residual diagnostic DNA and would complicate integration into routine pathological workflows. Sterile sampling would also require additional logistical efforts and would not be suitable for retrospective analyses. This study intentionally focused on residual DNA extracted from FFPE material to evaluate whether bacterial quantification can be implemented within routine molecular diagnostics.

In summary, this study demonstrates the possibility of detecting intratumoral bacterial DNA using molecular methods and highlights ddPCR as a particularly robust and sensitive approach for low-microbial biomass tumor sample analyses. For colorectal cancer samples, however, qPCR may represent a suitable and cost-effective alternative due to the typically higher bacterial DNA abundance. The observed association between bacterial load and inflammation underscores the potential relevance of intratumoral microbiota in shaping the immune tumor microenvironment, with possible consequences for treatment response and overall clinical outcome. Future studies with larger cohorts and standardized molecular workup will be required for a better understanding of the biological and clinical relevance of intratumoral bacteria. This could ultimately contribute to a more individualized approach to cancer treatment and open new therapeutic possibilities through modulation of bacterial communities within the TME.

6. References

1. Cancer (IARC) TIA for R on. Global Cancer Observatory [Internet]. [cited 2025 Dec 5]. Available from: https://gco.iarc.fr/

2. Islami F, Torre LA, Jemal A. Global trends of lung cancer mortality and smoking prevalence. Transl Lung Cancer Res. 2015 Aug;4(4):327–38.

3. Bray F, Laversanne M, Sung H, Ferlay J, Siegel RL, Soerjomataram I, et al. Global cancer statistics 2022: GLOBOCAN estimates of incidence and mortality worldwide for 36 cancers in 185 countries. CA Cancer J Clin. 2024;74(3):229–63.

4. Roshandel G, Ghasemi-Kebria F, Malekzadeh R. Colorectal Cancer: Epidemiology, Risk Factors, and Prevention. Cancers. 2024 Apr 17;16(8):1530.

5. Johannsen IR, Boysen AK, Mortensen FV, Kirkegård J. Temporal trends in incidence and mortality of colorectal cancer in Denmark from 2007 to 2022. Int J Cancer. 2025 Aug 15;157(4):634–43.

6. Arastéh K, editor. Innere Medizin. 5., vollständig überarbeitete Auflage. Stuttgart: Thieme; 2024. 453–461 p. (Duale Reihe).

7. Smolarz B, Łukasiewicz H, Samulak D, Piekarska E, Kołaciński R, Romanowicz H. Lung Cancer—Epidemiology, Pathogenesis, Treatment and Molecular Aspect (Review of Literature). Int J Mol Sci. 2025 Feb 26;26(5):2049.

8. TNM staging for lung cancer [Internet]. [cited 2026 Jan 8]. Available from: https://www.cancerresearchuk.org/about-cancer/lung-cancer/stages-types/tnm-staging

9. Adenocarcinoma overview [Internet]. [cited 2026 Feb 20]. Available from: https://www.pathologyoutlines.com/topic/lungtumoradenocarcinoma.html

10. Li Y, Li Y, Liu J, Fan Y, Li X, Dong M, et al. Expression levels of microRNA-145 and microRNA-10b are associated with metastasis in non-small cell lung cancer. Cancer Biol Ther. 2016;17(3):272–9.

11. Dong J, Li B, Lin D, Zhou Q, Huang D. Advances in Targeted Therapy and Immunotherapy for Non-small Cell Lung Cancer Based on Accurate Molecular Typing. Front Pharmacol. 2019;10:230.

12. Cohen JG, Reymond E, Jankowski A, Brambilla E, Arbib F, Lantuejoul S, et al. Lung adenocarcinomas: correlation of computed tomography and pathology findings. Diagn Interv Imaging. 2016 Oct;97(10):955–63.

13. Alidousty C, Baar T, Heydt C, Wagener-Ryczek S, Kron A, Wolf J, et al. Advance of theragnosis biomarkers in lung cancer: from clinical to molecular pathology and biology. J Thorac Dis. 2019 Jan;11(Suppl 1):S3–8.

14. Rudin CM, Poirier JT, Byers LA, Dive C, Dowlati A, George J, et al. Molecular subtypes of small cell lung cancer: a synthesis of human and mouse model data. Nat Rev Cancer. 2019 May;19(5):289–97.

15. Qu S, Fetsch P, Thomas A, Pommier Y, Schrump DS, Miettinen MM, et al. Molecular Subtypes of Primary SCLC Tumors and Their Associations With Neuroendocrine and Therapeutic Markers. J Thorac Oncol. 2022 Jan 1;17(1):141–53.

16. Sasaki T, Kuno H, Hiyama T, Oda S, Masuoka S, Miyasaka Y, et al. 2021 WHO Classification of Lung Cancer: Molecular Biology Research and Radiologic-Pathologic Correlation. Radiogr Rev Publ Radiol Soc N Am Inc. 2024 Mar;44(3):e230136.

17. Zhang Y, Vaccarella S, Morgan E, Li M, Etxeberria J, Chokunonga E, et al. Global variations in lung cancer incidence by histological subtype in 2020: a population-based study. Lancet Oncol. 2023 Nov;24(11):1206–18.

18. Sen T, Dotsu Y, Corbett V, Puri S, Sen U, Boyle TA, et al. Pulmonary neuroendocrine neoplasms: the molecular landscape, therapeutic challenges, and diagnosis and management strategies. Lancet Oncol. 2025 Jan;26(1):e13–33.

19. Zullo L, Filippiadis D, Hendriks LEL, Portik D, Spicer JD, Wistuba II, et al. Lung metastases. Nat Rev Dis Primer. 2025 Aug 21;11(1):60.

20. Liang X, Cheng Y, Zhou W, Ni J, Li Y, Feng G. Systematic Pan-Cancer Population-Based Analysis Reveals the Incidence and Prognosis of Lung Metastases at Diagnosis. J Oncol. 2021 June 15;2021:9999968.

21. Dubansky B, Lewis S, Telgenhoff D. Classification and Histological Characteristics of Colorectal Cancer. Am Soc Clin Lab Sci. 2023 Apr;36(2):50–4.

22. Labianca R, Beretta GD, Kildani B, Milesi L, Merlin F, Mosconi S, et al. Colon cancer. Crit Rev Oncol Hematol. 2010 May;74(2):106–33.

23. Colon carcinoma overview [Internet]. [cited 2026 Feb 20]. Available from: https://www.pathologyoutlines.com/topic/colontumorcarcinomageneral.html

24. Adenocarcinoma [Internet]. [cited 2026 Feb 20]. Available from: https://www.pathologyoutlines.com/topic/colontumoradenocarcinoma.html

25. Fleming M, Ravula S, Tatishchev SF, Wang HL. Colorectal carcinoma: Pathologic aspects. J Gastrointest Oncol. 2012 Sept;3(3):153–73.

26. Lee CT, Huang YC, Hung LY, Chow NH, Su PF, Ho CL, et al. Serrated adenocarcinoma morphology in colorectal mucinous adenocarcinoma is associated with improved patient survival. Oncotarget. 2017 May 23;8(21):35165–75.

27. Nagtegaal ID, Hugen N. The Increasing Relevance of Tumour Histology in Determining Oncological Outcomes in Colorectal Cancer. Curr Colorectal Cancer Rep. 2015 Oct 1;11(5):259–66.

28. Duma N, Santana-Davila R, Molina JR. Non–Small Cell Lung Cancer: Epidemiology, Screening, Diagnosis, and Treatment. Mayo Clin Proc. 2019 Aug;94(8):1623–40.

29. Piñeros M, Parkin DM, Ward K, Chokunonga E, Ervik M, Farrugia H, et al. Essential TNM: a registry tool to reduce gaps in cancer staging information. Lancet Oncol. 2019 Feb;20(2):e103–11.

30. O'Sullivan B, Brierley J, Byrd D, Bosman F, Kehoe S, Kossary C, et al. The TNM classification of malignant tumours—towards common understanding and reasonable expectations. Lancet Oncol. 2017 July;18(7):849–51.

31. Ghoreyshi N, Heidari R, Farhadi A, Chamanara M, Farahani N, Vahidi M, et al. Next-generation sequencing in cancer diagnosis and treatment: clinical applications and future directions. Discov Oncol. 2025 Apr 20;16:578.

32. Kulkarni NP, Tank SH, Korlekar PN, Shidhaye SS, Barve P. A review of gene mutations, conventional testing and novel approaches to cancer screening. Int J Exp Res Rev. 2023 Apr 30;30:134–62.

33. De Micheli V, Agnelli L, Conca E, Rabsiun Aramburu VL, Baggi A, Vingiani A, et al. Impact of comprehensive genomic profiling and molecular tumour board on costs and access to tailored therapies: real-world observational study. BMJ Open. 2025 May;15(5):e099134.

34. Lynch TJ, Bell DW, Sordella R, Gurubhagavatula S, Okimoto RA, Brannigan BW, et al. Activating Mutations in the Epidermal Growth Factor Receptor Underlying Responsiveness of Non–Small-Cell Lung Cancer to Gefitinib. N Engl J Med. 2004 May 20;350(21):2129–39.

35. Bouchard N, Daaboul N. Lung Cancer: Targeted Therapy in 2025. Curr Oncol. 2025 Mar;32(3):146.

36. Schmalz D, Krabóth Z, Czoma V, Urbán P, Gyenesei A, Ruzsics I, et al. Comprehensive Genomic Profiling of Small-Cell Lung Cancer Reveals Frequent Potentially Targetable Alterations. Int J Mol Sci. 2025 Jan;26(23):11512.

37. Pappas L, Quintanilha JCF, Huang RSP, Parikh AR. Genomic alterations associated with early-stage disease and early recurrence in patients with colorectal cancer. The Oncologist. 2025 Feb 6;30(2):oyae269.

38. Berner AM, Murugaesu N. The Evolving Role of Genomics in Colorectal Cancer. Clin Oncol. 2025 Jan 1;37:103661.

39. Paget S. The distribution of secondary growths in cancer of the breast. 1889. Cancer Metastasis Rev. 1989 Aug;8(2):98–101.

40. Visser KE de, Joyce JA. The evolving tumor microenvironment: From cancer initiation to metastatic outgrowth. Cancer Cell. 2023 Mar 13;41(3):374–403.

41. Wagner M, Wiig H. Tumor Interstitial Fluid Formation, Characterization, and Clinical Implications. Front Oncol. 2015 May 26;5:115.

42. Heldin CH, Rubin K, Pietras K, Östman A. High interstitial fluid pressure — an obstacle in cancer therapy. Nat Rev Cancer. 2004 Oct;4(10):806–13.

43. Quail D, Joyce J. Microenvironmental regulation of tumor progression and metastasis. Nat Med. 2013 Nov;19(11):1423–37.

44. Kyriazi AA, Karaglani M, Agelaki S, Baritaki S. Intratumoral Microbiome: Foe or Friend in Reshaping the Tumor Microenvironment Landscape? Cells. 2024 July 30;13(15):1279.

45. Maman S, Witz IP. A history of exploring cancer in context. Nat Rev Cancer. 2018 June;18(6):359–76.

46. Chuah S, Chew V. High-dimensional immune-profiling in cancer: implications for immunotherapy. J Immunother Cancer. 2020 Feb 6;8(1):e000363.

47. Jin MZ, Jin WL. The updated landscape of tumor microenvironment and drug repurposing. Signal Transduct Target Ther. 2020 Aug 25;5:166.

48. Warburg O, Wind F, Negelein E. THE METABOLISM OF TUMORS IN THE BODY. J Gen Physiol. 1927 Mar 7;8(6):519–30.

49. Valkenburg KC, de Groot AE, Pienta KC. Targeting the tumour stroma to improve cancer therapy. Nat Rev Clin Oncol. 2018 June;15(6):366–81.

50. Winkler J, Abisoye-Ogunniyan A, Metcalf KJ, Werb Z. Concepts of extracellular matrix remodelling in tumour progression and metastasis. Nat Commun. 2020 Oct 9;11:5120.

51. Wang W, Li L, Chen N, Niu C, Li Z, Hu J, et al. Nerves in the Tumor Microenvironment: Origin and Effects. Front Cell Dev Biol. 2020 Dec 17;8:601738.

52. Almeida A, Mitchell AL, Boland M, Forster SC, Gloor GB, Tarkowska A, et al. A new genomic blueprint of the human gut microbiota. Nature. 2019;568(7753):499–504.

53. Sender R, Fuchs S, Milo R. Revised Estimates for the Number of Human and Bacteria Cells in the Body. PLoS Biol. 2016 Aug 19;14(8):e1002533.

54. Liang G, Bushman FD. The human virome: assembly, composition and host interactions. Nat Rev Microbiol. 2021 Aug;19(8):514–27.

55. Hou K, Wu ZX, Chen XY, Wang JQ, Zhang D, Xiao C, et al. Microbiota in health and diseases. Signal Transduct Target Ther. 2022 Apr 23;7(1):135.

56. David LA, Maurice CF, Carmody RN, Gootenberg DB, Button JE, Wolfe BE, et al. Diet rapidly and reproducibly alters the human gut microbiome. Nature. 2014 Jan 23;505(7484):559–63.

57. Odamaki T, Kato K, Sugahara H, Hashikura N, Takahashi S, Xiao J zhong, et al. Age-related changes in gut microbiota composition from newborn to centenarian: a cross-sectional study. BMC Microbiol. 2016 May 25;16:90.

58. Laterza L, Rizzatti G, Gaetani E, Chiusolo P, Gasbarrini A. The Gut Microbiota and Immune System Relationship in Human Graft-versus-Host Disease. Mediterr J Hematol Infect Dis. 2016 May 1;8(1):e2016025.

59. Auchtung TA, Fofanova TY, Stewart CJ, Nash AK, Wong MC, Gesell JR, et al. Investigating Colonization of the Healthy Adult Gastrointestinal Tract by Fungi. mSphere. 2018 Mar 28;3(2):e00092-18.

60. Lozupone CA, Stombaugh JI, Gordon JI, Jansson JK, Knight R. Diversity, stability and resilience of the human gut microbiota. Nature. 2012 Sept 13;489(7415):220–30.

61. Dickson RP, Huffnagle GB. The Lung Microbiome: New Principles for Respiratory Bacteriology in Health and Disease. PLoS Pathog. 2015 July 9;11(7):e1004923.

62. Dickson RP, Erb-Downward JR, Martinez FJ, Huffnagle GB. The Microbiome and the Respiratory Tract. Annu Rev Physiol. 2016;78:481–504.

63. Leyden JJ, McGinley KJ, Mills OH, Kligman AM. Propionibacterium Levels In Patients With And Without Acne Vulgaris. J Invest Dermatol. 1975 Oct;65(4):382–4.

64. The Papyrus Ebers: The Greatest Egyptian Medical Document. Levin & Munksgaard; 1937. 152 p.

65. Sepich-Poore GD, Zitvogel L, Straussman R, Hasty J, Wargo JA, Knight R. The microbiome and human cancer. Science. 2021 Mar 26;371(6536):eabc4552.

66. Rous P. A SARCOMA OF THE FOWL TRANSMISSIBLE BY AN AGENT SEPARABLE FROM THE TUMOR CELLS. J Exp Med. 1911 Apr 1;13(4):397–411.

67. Epstein MA, Achong BG, Barr YM. VIRUS PARTICLES IN CULTURED LYMPHOBLASTS FROM BURKITT'S LYMPHOMA. Lancet Lond Engl. 1964 Mar 28;1(7335):702–3.

68. Dane DS, Cameron CH, Briggs M. Virus-like particles in serum of patients with Australia-antigen-associated hepatitis. Lancet Lond Engl. 1970 Apr 4;1(7649):695–8.

69. Beasley RP, Hwang LY, Lin CC, Chien CS. Hepatocellular carcinoma and hepatitis B virus. A prospective study of 22 707 men in Taiwan. Lancet Lond Engl. 1981 Nov 21;2(8256):1129–33.

70. zur Hausen H. Human papillomaviruses and their possible role in squamous cell carcinomas. Curr Top Microbiol Immunol. 1977;78:1–30.

71. Boshart M, Gissmann L, Ikenberg H, Kleinheinz A, Scheurlen W, zur Hausen H. A new type of papillomavirus DNA, its presence in genital cancer biopsies and in cell lines derived from cervical cancer. EMBO J. 1984 May;3(5):1151–7.

72. NobelPrize.org [Internet]. [cited 2026 Jan 8]. Nobel Prize in Physiology or Medicine 2008. Available from: https://www.nobelprize.org/prizes/medicine/2008/hausen/facts/

73. Marshall BJ, McGechie DB, Rogers PA, Glancy RJ. Pyloric Campylobacter infection and gastroduodenal disease. Med J Aust. 1985 Apr 15;142(8):439–44.

74. Umar Z, Tang JW, Marshall BJ, Tay ACY, Wang L. Rapid diagnosis and precision treatment of Helicobacter pylori infection in clinical settings. Crit Rev Microbiol. 2025 Mar;51(2):369–98.

75. de Martel C, Georges D, Bray F, Ferlay J, Clifford GM. Global burden of cancer attributable to infections in 2018: a worldwide incidence analysis. Lancet Glob Health. 2020 Feb;8(2):e180–90.

76. Biological agents. Volume 100 B. A review of human carcinogens. Iarc Monogr Eval Carcinog Risks Hum. 2012;100(PT B):1–441.

77. Liu X, Cheng Y, Zang D, Zhang M, Li X, Liu D, et al. The Role of Gut Microbiota in Lung Cancer: From Carcinogenesis to Immunotherapy. Front Oncol. 2021 Aug 19;11:720842.

78. Attebury H, Daley D. The gut microbiome and pancreatic cancer development and treatment. Cancer J Sudbury Mass. 2023;29(2):49–56.

79. Nazeer HA, Kannan S, Balakrishanan J, Nair VK, Kavitha Y, Bhosale NK. The gut microbiota and breast cancer: A comprehensive review of emerging links and therapeutic implications. Med Microecol. 2025 Dec 1;26:100155.

80. Nejman D, Livyatan I, Fuks G, Gavert N, Zwang Y, Geller LT, et al. The human tumor microbiome is composed of tumor type–specific intracellular bacteria. Science. 2020 May 29;368(6494):973–80.

81. Gihawi A, Wood HM, Clark J, O'Grady J, Eeles RA, Wedge DC, et al. The landscape of microbial associations in human cancer. Sci Transl Med. 2025 Sept 3;17(814):eads6166.

82. Anda M, Yamanouchi S, Cosentino S, Sakamoto M, Ohkuma M, Takashima M, et al. Bacteria can maintain rRNA operons solely on plasmids for hundreds of millions of years. Nat Commun. 2023 Nov 14;14(1):7232.

83. Islam RA, Rallis C. Ribosomal Biogenesis and Heterogeneity in Development, Disease, and Aging. Epigenomes. 2023 Aug 11;7(3):17.

84. Bartoš O, Chmel M, Swierczková I. The overlooked evolutionary dynamics of 16S rRNA revises its role as the “gold standard” for bacterial species identification. Sci Rep. 2024 Apr 20;14(1):9067.

85. Dubnau D, Smith I, Morell P, Marmur J. Gene conservation in Bacillus species. I. Conserved genetic and nucleic acid base sequence homologies. Proc Natl Acad Sci U S A. 1965 Aug;54(2):491–8.

86. Clarridge JE. Impact of 16S rRNA Gene Sequence Analysis for Identification of Bacteria on Clinical Microbiology and Infectious Diseases. Clin Microbiol Rev. 2004 Oct;17(4):840–62.

87. Woese CR. Bacterial evolution. Microbiol Rev. 1987 June;51(2):221–71.

88. Regueira-Iglesias A, Balsa-Castro C, Blanco-Pintos T, Tomás I. Critical review of 16S rRNA gene sequencing workflow in microbiome studies: From primer selection to advanced data analysis. Mol Oral Microbiol. 2023;38(5):347–99.

89. Saiki RK, Scharf S, Faloona F, Mullis KB, Horn GT, Erlich HA, et al. Enzymatic amplification of beta-globin genomic sequences and restriction site analysis for diagnosis of sickle cell anemia. Science. 1985 Dec 20;230(4732):1350–4.

90. Kralik P, Ricchi M. A Basic Guide to Real Time PCR in Microbial Diagnostics: Definitions, Parameters, and Everything. Front Microbiol. 2017 Feb 2;8:108.

91. Higuchi R, Dollinger G, Walsh PS, Griffith R. Simultaneous amplification and detection of specific DNA sequences. Biotechnol Nat Publ Co. 1992 Apr;10(4):413–7.

92. Vogelstein B, Kinzler KW. Digital PCR. Proc Natl Acad Sci U S A. 1999 Aug 3;96(16):9236–41.

93. Hindson BJ, Ness KD, Masquelier DA, Belgrader P, Heredia NJ, Makarewicz AJ, et al. High-Throughput Droplet Digital PCR System for Absolute Quantitation of DNA Copy Number. Anal Chem. 2011 Nov 15;83(22):8604–10.

94. Xu D, Zhang W, Li H, Li N, Lin JM. Advances in droplet digital polymerase chain reaction on microfluidic chips. Lab Chip. 2023;23(5):1258–78.

95. Alexander JL, Wilson ID, Teare J, Marchesi JR, Nicholson JK, Kinross JM. Gut microbiota modulation of chemotherapy efficacy and toxicity. Nat Rev Gastroenterol Hepatol. 2017 June;14(6):356–65.

96. Daillère R, Vétizou M, Waldschmitt N, Yamazaki T, Isnard C, Poirier-Colame V, et al. Enterococcus hirae and Barnesiella intestinihominis Facilitate Cyclophosphamide-Induced Therapeutic Immunomodulatory Effects. Immunity. 2016 Oct 18;45(4):931–43.

97. Iida N, Dzutsev A, Stewart CA, Smith L, Bouladoux N, Weingarten RA, et al. Commensal bacteria control cancer response to therapy by modulating the tumor microenvironment. Science. 2013 Nov 22;342(6161):967–70.

98. Amiri Khosroshahi R, Zeraattalab-Motlagh S, Sarsangi P, Nielsen SM, Mohammadi H. Effect of probiotic supplementation on chemotherapy- and radiotherapy-related diarrhoea in patients with cancer: an umbrella review of systematic reviews and meta-analyses. Br J Nutr. 2023 Nov 28;130(10):1754–65.

99. Guo H, Chou WC, Lai Y, Liang K, Tam JW, Brickey WJ, et al. Multi-omics analyses of radiation survivors identify radioprotective microbes and metabolites. Science. 2020 Oct 30;370(6516):eaay9097.

100. Vétizou M, Pitt JM, Daillère R, Lepage P, Waldschmitt N, Flament C, et al. Anticancer immunotherapy by CTLA-4 blockade relies on the gut microbiota. Science. 2015 Nov 27;350(6264):1079–84.

101. Sivan A, Corrales L, Hubert N, Williams JB, Aquino-Michaels K, Earley ZM, et al. Commensal Bifidobacterium promotes antitumor immunity and facilitates anti-PD-L1 efficacy. Science. 2015 Nov 27;350(6264):1084–9.

102. Chu S, Cheng Z, Yin Z, Xu J, Wu F, Jin Y, et al. Airway Fusobacterium is Associated with Poor Response to Immunotherapy in Lung Cancer. OncoTargets Ther. 2022;15:201–13.

103. Luu K, Ye JY, Lagishetty V, Liang F, Hauer M, Sedighian F, et al. Fecal and Tissue Microbiota Are Associated with Tumor T-Cell Infiltration and Mesenteric Lymph Node Involvement in Colorectal Cancer. Nutrients. 2023 Jan;15(2):316.

104. Bender MJ, McPherson AC, Phelps CM, Pandey SP, Laughlin CR, Shapira JH, et al. Dietary tryptophan metabolite released by intratumoral Lactobacillus reuteri facilitates immune checkpoint inhibitor treatment. Cell. 2023 Apr 27;186(9):1846-1862.e26.

105. Din MO, Danino T, Prindle A, Skalak M, Selimkhanov J, Allen K, et al. Synchronized cycles of bacterial lysis for in vivo delivery. Nature. 2016 Aug 4;536(7614):81–5.

106. Chowdhury S, Castro S, Coker C, Hinchliffe TE, Arpaia N, Danino T. Programmable bacteria induce durable tumor regression and systemic antitumor immunity. Nat Med. 2019 July;25(7):1057–63.

107. Zacharias M, Kashofer K, Wurm P, Regitnig P, Schütte M, Neger M, et al. Host and microbiome features of secondary infections in lethal covid-19. iScience [Internet]. 2022 Sept 16 [cited 2026 Jan 8];25(9). Available from: https://www.cell.com/iscience/abstract/S2589-0042(22)01198-1

108. Suzuki MT, Taylor LT, DeLong EF. Quantitative Analysis of Small-Subunit rRNA Genes in Mixed Microbial Populations via 5′-Nuclease Assays. Appl Environ Microbiol. 2000 Nov;66(11):4605–14.

109. Stankovic MM. Lung Microbiota: From Healthy Lungs to Development of Chronic Obstructive Pulmonary Disease. Int J Mol Sci [Internet]. 2025 Feb 7 [cited 2026 Feb 26];26(4). Available from: https://www.mdpi.com/1422-0067/26/4/1403

110. Hilmi M, Kamal M, Vacher S, Dupain C, Ibadioune S, Halladjian M, et al. Intratumoral microbiome is driven by metastatic site and associated with immune histopathological parameters: An ancillary study of the SHIVA clinical trial. Eur J Cancer. 2023 Apr 1;183:152–61.

111. Fang J, Wu M, Shen H, Liu W, Zhang T. Intratumoral microbial abundance and load influence the immune microenvironment of oral squamous cell carcinoma. Front Oncol. 2025 Sept 22;15:1616928.

112. Qiao H, Tan XR, Li H, Li JY, Chen XZ, Li YQ, et al. Association of Intratumoral Microbiota With Prognosis in Patients With Nasopharyngeal Carcinoma From 2 Hospitals in China. JAMA Oncol. 2022 Sept;8(9):1301–9.

113. Yao Y, Zhu Y, Chen K, Chen J, Li Y, Li D, et al. Microbiota in cancer: current understandings and future perspectives. Signal Transduct Target Ther. 2026 Feb 2;11(1):39.

114. Oosterlinck B, Ceuleers H, Arras W, De Man JG, Geboes K, De Schepper H, et al. Mucin-microbiome signatures shape the tumor microenvironment in gastric cancer. Microbiome. 2023 Apr 21;11:86.

115. Mima K, Nishihara R, Qian ZR, Cao Y, Sukawa Y, Nowak JA, et al. Fusobacterium nucleatum in colorectal carcinoma tissue and patient prognosis. Gut. 2016 Dec 1;65(12):1973–80.

116. Burns MB, Montassier E, Abrahante J, Priya S, Niccum DE, Khoruts A, et al. Colorectal cancer mutational profiles correlate with defined microbial communities in the tumor microenvironment. PLoS Genet. 2018 June 20;14(6):e1007376.

117. Liu E, Zhang F, Xu T, Ye L, Ma SSQ, Ji ZS. Relationship between tumor microbiota transcriptional activity and gene expression in breast cancer. BMC Cancer. 2023 Mar 16;23:252.

118. Liu W, Zhang X, Xu H, Li S, Lau HCH, Chen Q, et al. Microbial Community Heterogeneity Within Colorectal Neoplasia and its Correlation With Colorectal Carcinogenesis. Gastroenterology. 2021 June 1;160(7):2395–408.

119. Kostic AD, Gevers D, Pedamallu CS, Michaud M, Duke F, Earl AM, et al. Genomic analysis identifies association of Fusobacterium with colorectal carcinoma. Genome Res. 2012 Feb;22(2):292–8.

120. Hu J, Yang Y, Feng Y, Yu Y, Song X, Jia R. Association of Intratumoral Microbiota with Prognosis in Patients with Lacrimal Gland Tumor. Biomedicines. 2025 Apr 14;13(4):960.

121. Větrovský T, Baldrian P. The Variability of the 16S rRNA Gene in Bacterial Genomes and Its Consequences for Bacterial Community Analyses. PLoS ONE. 2013 Feb 27;8(2):e57923.

ChatGPT (GPT-5.3) was used exclusively for language editing where necessary, in accordance with the guidelines for good scientific practice of the Medical University of Graz (OpenAI, https://chatgpt.com).

7. Appendix

Supplementary Table S1a. Individual sample characteristics

Case No.	Category	Sex	Age (year)	Location	Primary location
1	CRC primary	M	71	RC	NA
2	CRC primary	F	56	LC	NA
3	CRC primary	F	38	RC	NA
4	CRC primary	M	81	LC	NA
5	CRC primary	F	80	RC	NA
6	CRC primary	M	70	RC	NA
7	CRC primary	F	66	RC	NA
8	Lung primary	F	67	LUL	NA
9	Lung primary	F	70	RLL	NA
10	Lung primary	M	78	LUL	NA
11	Lung primary	F	74	LLL	NA
12	Lung primary	M	78	LUL	NA
13	Lung primary	M	69	LUL	NA
14	Lung primary	M	72	RUL	NA
15	Metastasis	M	81	LUL	LC
16	Metastasis	M	59	LLL	LC
17	Metastasis	F	81	LUL	NA
18	Metastasis	M	66	RLL	LC
19	Metastasis	F	73	R lung (unspec.)	RC
20	Metastasis	M	54	RUL	LC
21	Metastasis	F	49	R lung (unspec.)	LC

Location refers to the anatomical tumor site of the case. Primary tumor location is reported for metastatic samples only.

Abbreviations: CRC (colorectal carcinoma), RC (right colon), LC (left colon), LUL (left upper lobe), LLL (left lower lobe), RUL (right upper lobe), RLL (right lower lobe), NA (not assessed).

Supplementary Table S1b. Individual sample characteristics

Case No.	T stage	N stage	Grade	DNA concentration *	Max. diameter ∇	Tumor cell content ◊
1	pT4b	pN1c	G3	188	60	60
2	pT3	pN0	G2	150	25	80
3	pT3	pN2b	NA	248	41	45
4	pT4a	pN1a	G3	104	45	50
5	pT4a	pN2b	G3	229	60	60
6	pT4a	pN1b	G2	222	30	80
7	pT4a	pN2b	G3	172	NA	60
8	pT2c	pN2	G3	176	28	50
9	pT2a	pN0	G3	290	25	40
10	pT1c	NA	G2	161	28	50
11	pT2a	pN2	G3	159	24	60
12	pT3	pN1	G3	211	55	70
13	pT1b	pN0	G2	215	16	70
14	pT4	pN0	G3	279	75	80
15	NA	NA	NA	163	11	60
16	NA	NA	NA	400	12	50
17	NA	NA	NA	228	32	30
18	NA	NA	NA	252	8	30
19	NA	NA	NA	218	13	30
20	NA	NA	NA	78	15	40
21	NA	NA	NA	228	8	80

T and N stages are reported according to the TNM classification.

** DNA concentration in ng/µL.*

∇ Maximum diameter in mm.

◊ Tumor cell content in %.

Abbreviations: NA (not assessed)

Supplementary Table S2. Mutation status of all analyzed genes

Gene	Mutated, n	Wild-type, n	NA, n
KRAS	11	10	0
BRAF	1	18	2
APC	0	18	3
EGFR	1	17	3
TP53	11	10	0
PIK3CA	5	13	3
SMAD4	0	18	3
FBXW7	1	17	3
CTNNB1	0	18	3
NRAS	1	18	2
HRAS	0	18	3
ERBB2	1	18	2
ERBB4	1	17	3
PTEN	0	18	3
ALK	1	17	3
MAP2K1	1	17	3
FGFR2	0	18	3
FGFR3	1	18	2
KEAP1	0	18	3
STK11	0	18	3
CDKN2A	0	18	3
Gene Fusion*	1*	6	14

**EML4::ALK*

Supplementary Table S3. qPCR results

Sample	Cq	Cq Mean	SQ	SQ Mean	SQ SD	SQ Mean (log10)
NTC-01	31.89	33.62				
NTC-02	33.9	33.62				
NTC-03	37.22	33.62				
NTC-04	31.46	33.62				
Pos Ctrl-01	8.37	8.48	2.89E+06	2.70E+06	1.62E+05	6.43
Pos Ctrl-01	8.55	8.48	2.58E+06	2.70E+06	1.62E+05	6.43
Pos Ctrl-01	8.52	8.48	2.63E+06	2.70E+06	1.62E+05	6.43
Std-01	6.34	9.99	1.00E+07	1.00E+07	0.00E+00	7
Std-01	17.12	9.99	1.00E+07	1.00E+07	0.00E+00	7
Std-01	6.52	9.99	1.00E+07	1.00E+07	0.00E+00	7
Std-02	9.71	9.58	1.00E+06	1.00E+06	0.00E+00	6
Std-02	9.53	9.58	1.00E+06	1.00E+06	0.00E+00	6
Std-02	9.51	9.58	1.00E+06	1.00E+06	0.00E+00	6
Std-03	13.63	13.64	1.00E+05	1.00E+05	0.00E+00	5
Std-03	13.61	13.64	1.00E+05	1.00E+05	0.00E+00	5
Std-03	13.69	13.64	1.00E+05	1.00E+05	0.00E+00	5
Std-04	18.61	18.22	1.00E+04	1.00E+04	0.00E+00	4
Std-04	17.02	18.22	1.00E+04	1.00E+04	0.00E+00	4
Std-04	19.03	18.22	1.00E+04	1.00E+04	0.00E+00	4
Std-05	21.8	21.83	1.00E+03	1.00E+03	0.00E+00	3
Std-05	21.77	21.83	1.00E+03	1.00E+03	0.00E+00	3
Std-05	21.93	21.83	1.00E+03	1.00E+03	0.00E+00	3
Std-06	24.78	24.93	1.00E+02	1.00E+02	0.00E+00	2
Std-06	24.49	24.93	1.00E+02	1.00E+02	0.00E+00	2
Std-06	25.52	24.93	1.00E+02	1.00E+02	0.00E+00	2
Std-07	27.79	27.95	1.00E+01	1.00E+01	0.00E+00	1
Std-07	28	27.95	1.00E+01	1.00E+01	0.00E+00	1
Std-07	28.06	27.95	1.00E+01	1.00E+01	0.00E+00	1
Sample 1	21.5	21.99	872.88	661.59	183.94	2.82
Sample 1	22.23	21.99	554.22	661.59	183.94	2.82
Sample 1	22.22	21.99	557.68	661.59	183.94	2.82

Sample 2	26.37	26.64				
Sample 2	27.92	26.64				
Sample 2	25.63	26.64				
Sample 3	22.57	22.58	448.54	446.83	13.9	2.65
Sample 3	22.53	22.58	459.85	446.83	13.9	2.65
Sample 3	22.63	22.58	432.11	446.83	13.9	2.65
Sample 4	23.56	23.42	242.25	241.5	1.06	2.38
Sample 4	23.12	23.42		241.5	1.06	2.38
Sample 4	23.57	23.42	240.75	241.5	1.06	2.38
Sample 5	31.3	27.06		106.01	37.44	2.03
Sample 5	25.35	27.06	79.53	106.01	37.44	2.03
Sample 5	24.53	27.06	132.48	106.01	37.44	2.03
Sample 6	ND					
Sample 6	ND					
Sample 6	ND					
Sample 7	20.66	20.68	1472.14	1451.23	36.23	3.16
Sample 7	20.66	20.68	1472.14	1451.23	36.23	3.16
Sample 7	20.73	20.68	1409.4	1451.23	36.23	3.16
Sample 8	27.63	26.04				
Sample 8	24.8	26.04				
Sample 8	25.68	26.04				
Sample 9	28.6	28.64				
Sample 9	29.63	28.64				
Sample 9	27.68	28.64				
Sample 10	26.85	27.73		13.81	2.24	1.14
Sample 10	27.99	27.73	15.39	13.81	2.24	1.14
Sample 10	28.36	27.73	12.22	13.81	2.24	1.14
Sample 11	ND					
Sample 11	ND					
Sample 11	ND					
Sample 12	26.9	27.15	30.32	29.41	1.29	1.47
Sample 12	27.54	27.15		29.41	1.29	1.47
Sample 12	27	27.15	28.49	29.41	1.29	1.47
Sample 13	ND					

Sample 13	ND					
Sample 13	ND					
Sample 14	28.34	28.19	12.38	13.9	3.35	1.14
Sample 14	28.45	28.19	11.56	13.9	3.35	1.14
Sample 14	27.76	28.19	17.75	13.9	3.35	1.14
Sample 15	26.69	26.85	34.55	35.78	1.73	1.55
Sample 15	27.3	26.85		35.78	1.73	1.55
Sample 15	26.58	26.85	37	35.78	1.73	1.55
Sample 16	ND					
Sample 16	ND					
Sample 16	ND					
Sample 17	ND					
Sample 17	ND					
Sample 17	ND					
Sample 18	31.18	30.81	2.11	2.73	0.88	0.44
Sample 18	ND			2.73	0.88	0.44
Sample 18	30.44	30.81	3.35	2.73	0.88	0.44
Sample 19	ND			1.44	0.52	0.16
Sample 19	31.43	31.85	1.81	1.44	0.52	0.16
Sample 19	32.27	31.85	1.07	1.44	0.52	0.16
Sample 20	22.33	21.84	520.79	723.82	175.79	2.86
Sample 20	21.59	21.84	825.34	723.82	175.79	2.86
Sample 20	21.59	21.84	825.34	723.82	175.79	2.86
Sample 21	ND					
Sample 21	ND					
Sample 21	ND					

If one of the technical triplicates failed to yield a reliable amplification signal, this replicate was excluded and no SQ value was calculated for that replicate.
Abbreviations: NTC (no-template control), ND (not detected), SD (standard deviation)

Supplementary Table S4. ddPCR results		
Case Nr.	**16S copies**	**log10 16s copies**
1	52774.27	4.72
2	1326.82	3.12
3	28075.40	4.45
4	739.48	2.87
5	2092.43	3.32
6	2582.72	3.41
7	140155.31	5.15
8	48.84	1.69
9	62.53	1.80
10	153.23	2.19
11	84.77	1.93
12	93.20	1.97
13	68.06	1.83
14	38.04	1.58
15	101.67	2.01
16	185.24	2.27
17	161.92	2.21
18	54.30	1.74
19	113.03	2.05
20	19991.44	4.30
21	917.18	2.96

Supplementary Table S5. Individual histological scores

Case No.	Category	Necrosis (%)	Mucin (%)	Inflammation (%)
1	Colon primary	25%	0%	5%
2	Colon primary	5%	1%	5%
3	Colon primary	1%	1%	5%
4	Colon primary	20%	5%	25%
5	Colon primary	5%	5%	5%
6	Colon primary	10%	20%	5%
7	Colon primary	20%	5%	10%
8	Lung primary	10%	10%	10%
9	Lung primary	5%	5%	40%
10	Lung primary	0%	0%	10%
11	Lung primary	10%	5%	10%
12	Lung primary	50%	10%	5%
13	Lung primary	1%	40%	10%
14	Lung primary	10%	5%	30%
15	Metastasis	30%	0%	10%
16	Metastasis	50%	1%	5%
17	Metastasis	40%	25%	10%
18	Metastasis	35%	5%	15%
19	Metastasis	10%	10%	25%
20	Metastasis	75%	1%	5%
21	Metastasis	75%	1%	5%

Values are given as percentage of total tumor area.